

5

Optical, Ultraviolet and Infrared Observations of X-ray Binaries

P.A. CHARLES and M.J. COE
*School of Physics & Astronomy, University of Southampton,
 Highfield, Southampton SO17 1BJ, UK*

5.1 Introduction

In the 35 years since the first X-ray binary was optically identified (Sco X-1) the basic division of X-ray binaries into the high-mass (HMXBs) and low-mass (LMXBs) systems has become firmly established. The nomenclature refers to the nature of the mass donor, with HMXBs normally taken to be $\geq 10M_{\odot}$, and LMXBs $\leq 1M_{\odot}$. However, the last decade has seen the identification and measurement of a significant number of X-ray binaries whose masses are intermediate between these limits. Nevertheless, the nature of the mass-transfer process (stellar wind dominated in HMXBs, Roche lobe overflow in LMXBs) produces quite different properties in the two groups and so this chapter will be divided into two main sections on HMXBs and LMXBs. A more complete Introduction can be found in chapter 1.

While the nature of the compact object and its properties are largely determined from X-ray studies (e.g. chapters 1,4), longer-wavelength observations allow detailed studies of the properties of the mass donor. This is most straight-forward for the intrinsically luminous early-type companions of HMXBs, which provides the potential for a full solution of the binary parameters for those systems containing X-ray pulsars. This is particularly important for HMXB evolution in that it allows a comparison of the derived masses with those obtained for neutron stars in the much older binary radio pulsar systems (Thorsett & Chakrabarty, 1999).

However, when HMXBs are suspected of harbouring black holes (e.g. Cyg X-1), the mass measurement process runs into difficulties. By definition, there will be no kinematic features (such as pulsations) associated with the compact object, and hence the analysis is based entirely on the mass-losing companion. Most importantly, the mass of the compact object depends on the accuracy to which that of the companion is known. The situation for LMXBs, such as Sco X-1, is completely different, in that their short orbital periods require their companion stars to be of much lower mass. In section 5.3 we collect together and discuss the results of mass determinations in all X-ray binaries. We also emphasise those properties that LMXBs have in common with cataclysmic variables (chap 10), most of which are related to the similar structure of their accretion discs.

More recently, the advent of near-IR spectroscopic instrumentation on large telescopes has allowed the first detailed investigations of X-ray binaries in the Galactic Bulge and other regions of high extinction.

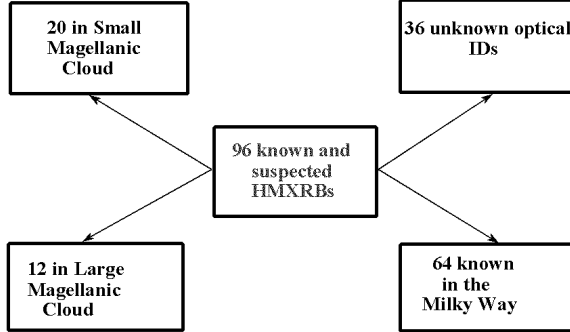


Fig. 5.1. Distribution of different HMXB populations

5.2 HIGH-MASS X-RAY BINARIES

5.2.1 Supergiant and Be X-ray binaries

There are two main sub-groups of HMXBS - the supergiant counterparts (normally of luminosity class I or II), and the Be/X-ray (or BeX) binary systems (normally luminosity class III or V). Both sub-groups involve OB type stars and are commonly found in the galactic plane and the Magellanic Clouds. They differ, however, in accretion modes with the supergiant systems accreting from a radially outflowing stellar wind, and the BeX binaries accreting directly from the circumstellar disc (possibly with some limited Roche lobe overflow on rare occasions). As a result the supergiants are persistent sources of X-rays, whilst the BeX systems are very variable and frequently much brighter.

Recently Reig & Roche (1999) have suggested a third sub-group of systems; the X Per like systems. Their main characteristics are: long pulse periods (typically 1000s), persistent low L_x ($\sim 10^{34}$ erg/s) and low variability, and rare uncorrelated weak X-ray outbursts. The properties of all three groups are summarised in Table 5.1.

Currently (August 2003) there are about 100 known or suspected HMXBs (see Figure 5.1). Surprisingly, nearly one third of these lie in the Magellanic Clouds. This very large fraction, particularly noticeable in the SMC, will be discussed later. About one third of all the HMXBs have no known optical counterpart, simply due to the historical inaccuracy of the X-ray location. Current facilities such as the *Chandra X-ray Observatory* are very effective tools to rectify this situation.

Progress towards a better understanding of the physics of these systems depends on multi-wavelength studies. From observations of the Be star in the optical, UV and IR, the physical conditions under which the neutron star is accreting can be determined. In combination with hard X-ray timing observations, this yields a near complete picture of the accretion process. It is thus vital to identify the optical counterparts and obtain UV to IR measurements for these X-ray systems in order to further our understanding.

Table 5.1. *General properties of HMXBs.*

Type*	Percent of all HMXB	Optical Luminosity Class	Typical pulse period(s)	Typical binary period(d)	Typical binary eccentricity	Log L_X (erg s ⁻¹)
Be	57	III-V	0.05-500	2-260	0.3-0.9	36-38
SG	25	I-II	200-700	3-40		34-35
XP	10	III-V	200-1400	250	0.03	34-35
Others	8	-	-	-	-	

* Be = Be star binaries, SG = supergiant systems, XP = systems similar to X Per

5.2.2 Be/X-ray binaries

The BeX binary systems represent the largest sub-class of HMXBs. Of 96 currently proposed HMXB pulsars, 57% are identified as BeX type. The orbit of the Be or supergiant star and the compact object, presumably a neutron star, is generally wide and eccentric. X-ray outbursts are normally associated with the passage of the neutron star through the circumstellar disc. The physics of accretion-powered pulsars has been reviewed previously (e.g. White, Nagase & Parmar 1995, Nagase 1989, Bildsten et al 1997). This section will concentrate on the optical, UV and IR observational properties of BeX systems and address how these have contributed to our understanding of Be star behaviour.

X-ray behavioural features of BeX systems include:

- regular periodic outbursts at periastron (*Type I*);
- giant outbursts at any phase probably arising from a dramatic expansion of the circumstellar disc (*Type II*);
- “missed” outbursts frequently related to low H α emission levels (hence a small disc), or other unknown reasons (e.g. perhaps centrifugal inhibition of accretion, see Stella, White & Rosner 1986);
- shifting outburst phases due to the rotation of density structures in the circumstellar disc (Wilson et al, 2002).

For supergiant systems the X-ray characteristics tend to be much less dramatic. Because of the predominantly circular orbits and the much steadier wind outflow, the X-ray emission tends to be a regular low-level effect. Rarely Type II outbursts may occur, but never Type I.

One particularly interesting piece of astrophysics emerged early on in the study of BeX systems - the Corbet diagram (Corbet 1986). This diagram showed a strong correlation between their orbital and pulse periods. An updated version of this diagram is presented in Figure 5.2. For a system to be detected as an X-ray source it is necessary that the pressure of infalling material be sufficient to overcome centrifugal inhibition. In other words, the Alfvén radius must be inside the magnetospheric boundary. For BeX systems the correlation is understood in terms of the wider orbits exposing the neutron stars to a lower wind density on average and hence weaker accretion pressures. Thus it is only those systems that have a correspondingly

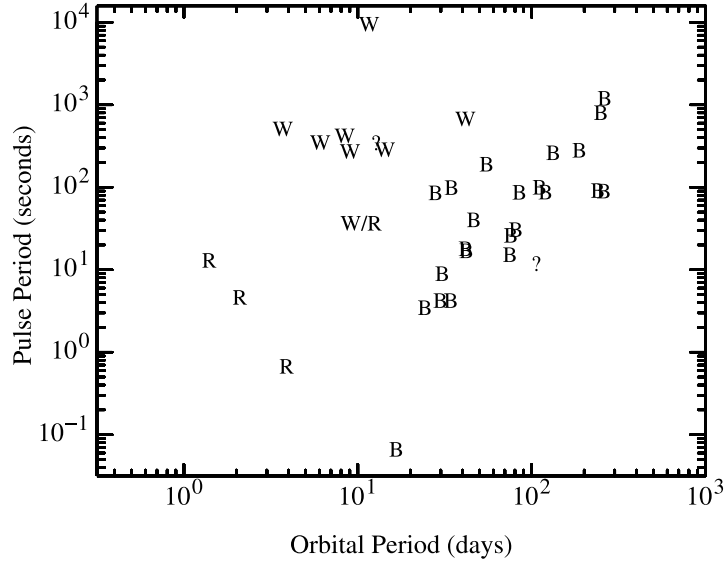


Fig. 5.2. An updated version of the Corbet diagram (Corbet 1986) provided by Corbet (private communication). The three classes of object illustrated are: B = BeX binaries, W = wind-fed, R = Roche-lobe overflow. Two systems are indicated by ? symbols because their optical properties are not yet clear.

weaker centrifugal inhibition (i.e. slower spin rates) that permit accretion to occur and hence permit their possible discovery as an X-ray source.

A powerful feature of this diagram is that it allows one to predict either the pulse, or the binary period, if one knows the other parameter. Alternatively, if both periods are determined (from e.g. X-ray measurements) then the class of object may be defined, even in the absence of an optical counterpart.

5.2.3 *Magellanic Cloud HMXBs*

It has come as a great surprise to discover that there are a large number of BeX binaries in the SMC. Figure 5.3 shows the distribution of almost all the known HMXB pulsars superimposed upon an HI image of the SMC.

It is possible to estimate the number of systems one would expect based upon the relative masses of our Galaxy and the SMC. This ratio is ~ 50 , so with 64 known or suspected systems in our Galaxy we would only expect 1 or 2 in the SMC. However, Maeder et al(1999) have shown that the fraction of Be to B stars is 0.39 in the SMC compared with 0.16 in our Galaxy. So this raises the expected number of BeX systems to ~ 3 - but we now know of ≥ 35 (Table 5.2)!

The answer almost certainly lies in the history of the Magellanic Clouds. Detailed HI mapping by Staveley-Smith et al (1997) and Putman et al (1998) has shown the existence of a significant bridge of material between the Magellanic Clouds and

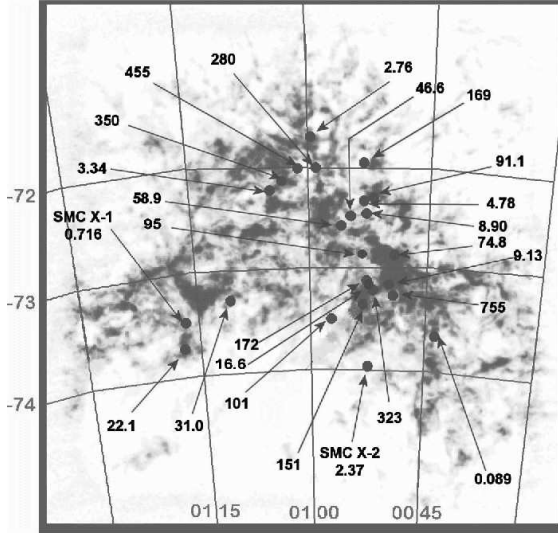


Fig. 5.3. An HI image of the SMC (Stanimirovic et al, 1999), on which is superposed the location of 25 known X-ray binary pulsars. The numbers indicate their pulse period in seconds.

between them and our own Galaxy. Furthermore, Staveland-Smith et al have demonstrated the existence of a large number of supernova remnants of similar age (~ 5 Myr), strongly suggesting enhanced starbirth has taken place as a result of tidal interactions between these component systems. Consequently it seems very likely that the previous closest approach of the SMC to the LMC ~ 100 Myrs ago may have triggered the birth of many new massive stars which have given rise to the current population of HMXBs. In fact, other authors (e.g. Popov et al 1998) claim that the presence of large numbers of HMXBs may be the best indication of starburst activity in a system.

Excellent support for this interpretation comes from both the work of Meyssonnier & Azzopardi (1993) in cataloguing emission line stars, and the work of Maragoudaki et al (2001) in identifying stars of age in the range 8-12 My. Figure 5.4 shows the results of both of these surveys and demonstrates a strong spatial correlation with the distribution of X-ray pulsars shown in Figure 5.3.

As a result, the SMC now provides us with an excellent sample of BeX systems in a relatively compact and easily observable region of the sky. In addition the similarity between the population sizes seen in the Galaxy (~ 50) and the SMC (~ 30) permits interesting comparisons to be made. Figure 5.5 from Laycock et al (2003) shows the binned population distributions per decade in period and normalised to unity. Applying the K-S test to the two populations gives a probability of 97% that the two samples were drawn from different distributions (although varying extinction conditions may significantly affect the homogeneity of the galactic population).

In complete contrast, the HMXB population of the LMC seems very representative of the sample found in the Milky Way. A comprehensive review by Negueruela &

Table 5.2. *Properties of X-ray pulsars in the SMC*

Short name	Full or alternative name(s)	Spectral Class	V mag	Period secs
SXP0.09	AX J0043-737	Be?		0.087
SXP0.72	SMC X-1	B0Ib	13.25	0.716
SXP0.92	PSR0045-7319	B	16.00	0.92
SXP2.16	XTE SMC pulsar			2.16
SXP2.37	SMC X-2	B1.5V	16.00	2.37
SXP2.76	RX J0059.2-7138	B1III	14.10	2.76
SXP3.34	AX J0105-722, RX J0105.3-7210			3.343
SXP4.78	XTE J0052-723, [MA93]537		15.80	4.782
SXP5.44	CXOU J010042.8-721132	AXP?	17.80	5.44
SXP7.70	XTE SMC pulsar			7.7
SXP8.90	RX J0051.8-7231, 1E0050.1-7247	B1III-V		8.9
SXP9.13	AX J0049-732			9.132
SXP15.3	RX J0052.1-7319	B1III - B0V	14.70	15.3
SXP16.6	RX J0051.8-7310			16.6
SXP22.1	RX J0117.6-7330	B0.5III	14.20	22.07
SXP31.0	XTE J0111.2-7317	O8-B0V	15.35	31
SXP46.4	XTE SMC pulsar			46.4
SXP46.6	1WGA 0053.8-7226, XTE J0053-724	B1-2III-V	14.90	46.6
SXP51.0	XTE SMC pulsar			51
SXP58.9	RX J0054.9-7226, XTE J0055-724			58.95
SXP74.8	RX J0049.1-7250, AX J0049-729	Be ?	15.90	74.8
SXP82.4	XTE J0052-725			82.4
SXP89.0	XTE SMC pulsar			89
SXP91.1	AX J0051-722, RX J0051.3-7216		15.00	91.1
SXP95.2	XTE SMC pulsar			95.2
SXP101	AX J0057.4-7325, RX J0057.3-7325			101.4
SXP152	CXOU J005750.3-720756, [MA93]1038			152.1
SXP164	XTE SMC pulsar			164.7
SXP169	XTE J0054-720, AX J0052.9-7158		15.50	169.3
SXP172	AX J0051.6-7311, RX J0051.9-7311			172.4
SXP280	AX J0058-72.0			280.4
SXP304	CXOU J010102.7-720658, [MA93]1240			304.5
SXP323	AX J0051-73.3, RXJ0050.7-7316	B0-B1V	15.40	323.2
SXP349	SAX J0103.2-7209, RX J0103-722	O9-B1III-V	14.80	349.9
SXP455	RX J0101.3-7211			455
SXP564	CXOU J005736.2-721934, [MA93]1020			564.8
SXP755	AX J0049.4-7323, RX J0049.7-7323	B1-3V		755.5

Coe (2002) of all identified optical counterparts in the LMC found that the overall spectral distribution of the population looks very similar to that of our Galaxy (Figure 5.6). They found that the spectral distribution for BeX binaries in both the

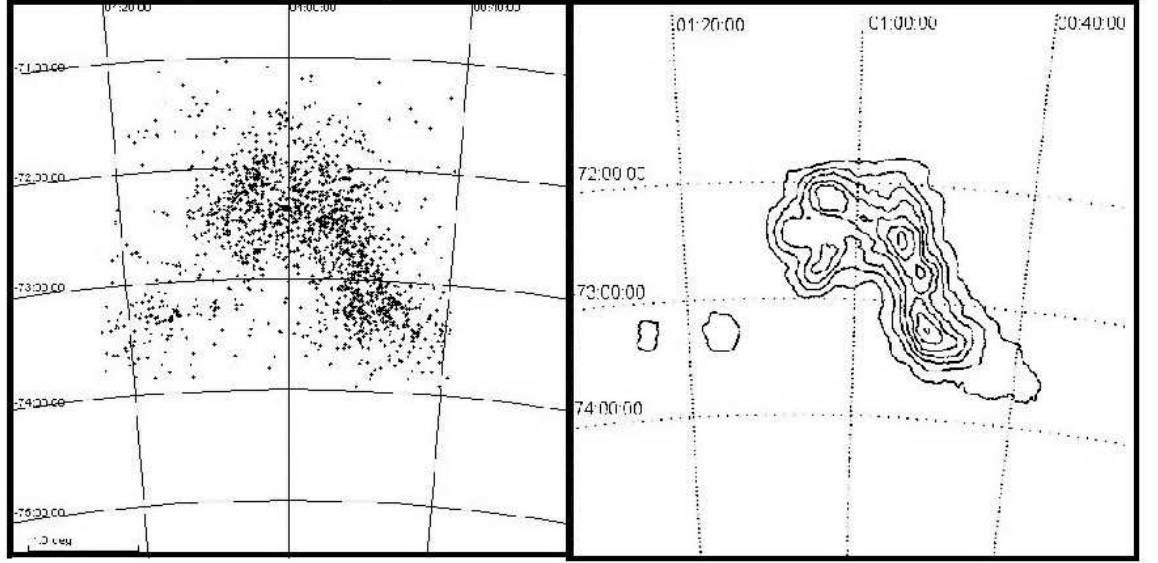


Fig. 5.4. Left: spatial distribution of emission line stars in the SMC Meyssonnier & Azzopardi (1993). Right: isodensity contours for SMC stars aged 8-12 Myr Maragoudaki et al (2001).

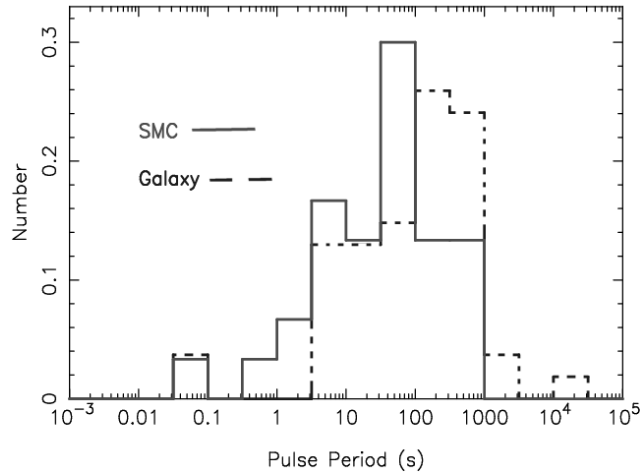


Fig. 5.5. Comparison of the X-ray pulsar population of the Galaxy and SMC (Laycock et al, 2003).

Milky Way and the LMC is sharply peaked at spectral type B0 (roughly corresponding to $M_* \approx 16M_\odot$) and not extending beyond B2 ($M_* \approx 10M_\odot$), which strongly supports the existence of supernova kicks. So the BeX binaries in the LMC must have preferentially formed from moderately massive binaries undergoing semi-conservative evolution in the same manner as most galactic systems.

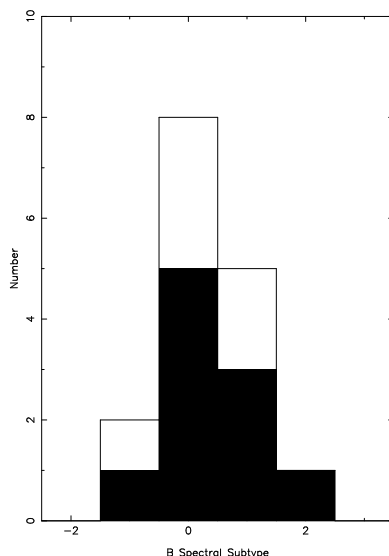


Fig. 5.6. Comparison of the X-ray pulsar optical counterparts in the Galaxy (white) and LMC (black) Negueruela & Coe (2002). Negative spectral types represent O-type stars.

5.2.4 *Properties of BeX circumstellar discs*

Typically the optical star exhibits $H\alpha$ line emission and continuum free-free emission (revealed as excess IR flux) from a disc of circumstellar gas. Therefore $H\alpha$ measurements provide very useful information on the disc's physical state. A1118-616 provides an excellent example of a classic BeX system that can be probed effectively in $H\alpha$. Discovered by chance in 1974 while *Ariel 5* was observing the nearby source Cen X-3 (Eyles et al, 1975), the flux increased by more than an order of magnitude during the outburst and became the dominant hard X-ray source in the Centaurus region for 7-10 days. The system then disappeared for 27 years before re-emerging in the same dramatic style in 1991 (Coe et al 1994).

The explanation for these sudden massive X-ray outbursts on very long timescales lies in the $H\alpha$ observations carried out prior to, during, and after the 1991 outburst. Note, no similar observations exist for the 1974 outburst since the optical counterpart was not identified at that time. The history of the $H\alpha$ observations over a 10 year period are shown in Figure 5.7, from which it is immediately apparent why A1118-616 went into outburst when it did - the $H\alpha$ equivalent width had reached an exceptionally high value $\geq 100\text{\AA}$. Since the pulse period is 404s the Corbet diagram (Corbet 1986) suggests P_{orb} in the range 200-300d, therefore it is extremely unlikely that the two recorded outbursts relate to binary motion (Type I outbursts).

It is far more likely that these are Type II outbursts, and the normal Type I outbursts are either very minor or absent. This could simply be due to the orbit not normally taking the neutron star through the circumstellar disc. However, during these abnormal levels of $H\alpha$ activity, the disc probably expands to include the neutron star's orbit, and hence accretion immediately begins. Note the strikingly rapid

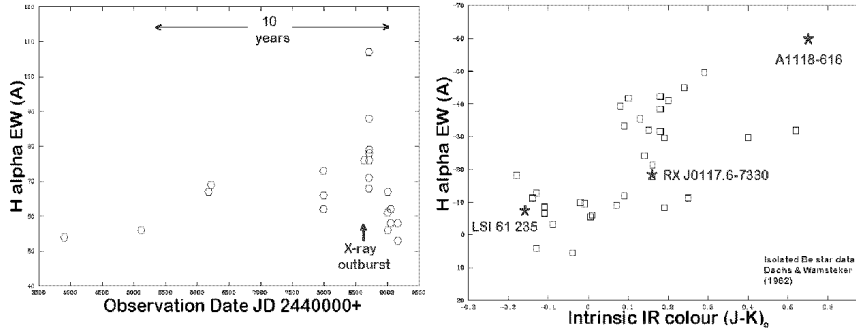


Fig. 5.7. Left - the history of the H α emission from A1118-616 showing the large rise coincident with the X-ray outburst. Right - The relationship between the intrinsic IR colours and H α equivalent width. Three BeX systems are compared to a set of isolated Be stars (Coe et al, 1994).

decline of H α immediately after the outburst suggesting that the whole period of activity was probably just due to one major mass ejection event from the Be star.

It is interesting to compare the size of the circumstellar disc seen in A1118-616 with that observed in other systems. Figure 5.7 shows a plot of H α EW against the intrinsic IR colour (also thought to arise from free-free and free-bound emission in the circumstellar disc), and an obvious and unsurprising correlation clearly exists between these two parameters. The quiescent location of A1118-616 is shown together with two other BeX systems, and compared with data from a sample of isolated Be stars (Dachs et al, 1982). It is interesting to note, that even in quiescence, A1118-616 is at the extreme edge of the diagram, and in fact, its peak H α EW value of $\sim 110\text{\AA}$ may be one of the very largest recorded values for any Be star.

With one notable exception discussed below, the H α profiles follow the behavioural patterns seen in isolated Be stars. The profile shape is dominated by the circumstellar disc structure and its inclination to our line of sight. A range of possible profiles are observed and these are well documented and classified elsewhere (eg Hanuschik et al 1988, Hanuschik 1996). A good example of a set of varying H α profiles from X Per is shown in Figure 5.8 (Clark et al, 2001). Not only does this range of profiles indicate significant variations in disc size, there is strong evidence that the blue and red components are varying with respect to each other - known as V/R variations. These V/R changes can only be explained by non-uniformities in the disc structure which are rotating around the system.

The structure of these discs has been explained by Okazaki & Negueruela, 2001 and others. They have investigated the tidal torques on these circumstellar (or “decretion” discs and found that a natural truncation occurs at certain resonance points (radii at which the local Keplerian period is an integer fraction of the orbital period). Beyond this truncation point matter cannot be transported. Furthermore, HMXBs with very circular orbits are truncated at a fixed size all the time, often smaller than the Roche lobe, making accretion on to the neutron star very unlikely. As a result these systems tend to only exhibit persistent low-level X-ray emission from the stellar wind plus occasional Type II outbursts. Conversely, systems with high

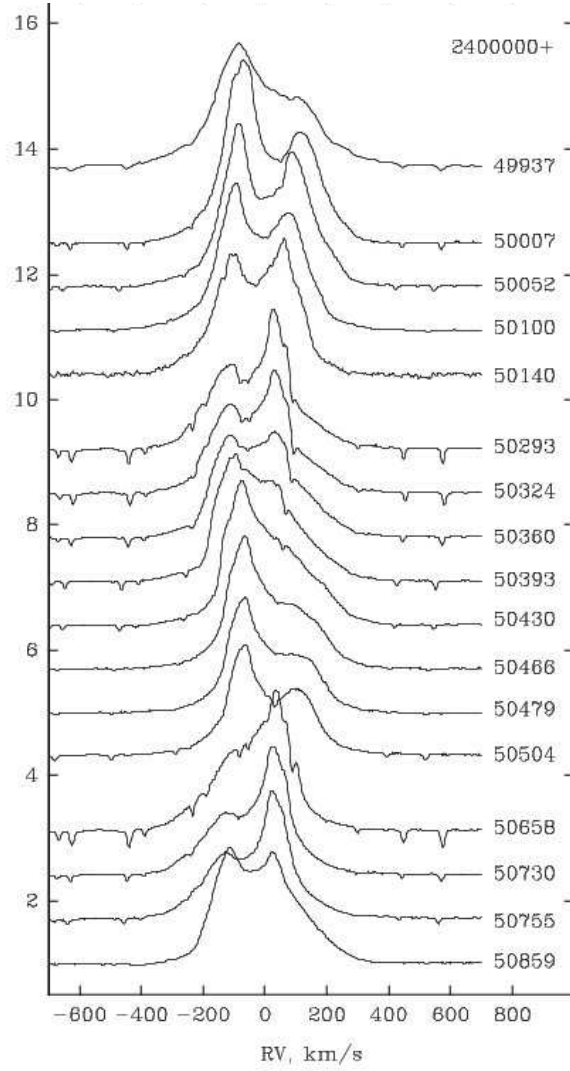


Fig. 5.8. Normalised $H\alpha$ profiles of X Per as a function of velocity relative to the rest wavelength. Different dates given on the right hand side of the figure. From Clark et al (1994).

eccentricities permit the size of the disc to be orbital-phase dependant and during periastron passage the disc can extend well into the orbital path of the neutron star triggering a Type I X-ray outburst.

Finally, direct $H\alpha$ imaging has shown itself to be a powerful tool in determining the environment around HMXBs in the case of Vela X-1. The spectacular image reported by Kaper et al 1997 (reproduced here as Figure 5.9) provides direct evidence of a bow shock around this system. This is clear indication that Vela X-1 is travelling at supersonic velocities through the ISM. Kaper et al used the symmetry of the

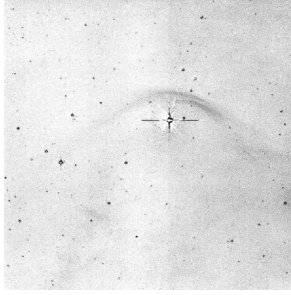


Fig. 5.9. 9' x 9' H α image of the Vela X-1 bow shock (Kaper et al 1997).

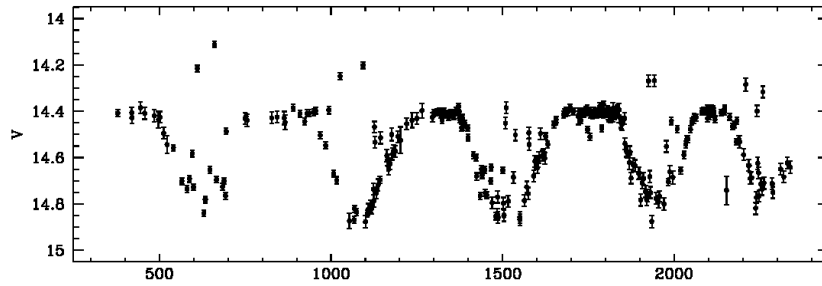


Fig. 5.10. The 5.5yr MACHO optical light curve for A0538-66 showing a regular modulation at $P=421$ d. From McGowan & Charles (2003).

shock to derive the direction of motion and the origin and age of the system. Their results support the Blaauw scenario (Blaauw 1961) whereby a supernova explosion of one binary component can result in a high space velocity of the companion (an “OB runaway”). Surprisingly, this runaway star has a high probability of remaining bound to its companion and thereby producing systems like Vela X-1.

5.2.5 Long-term optical monitoring

Of great value in the study of BeX systems has been the availability of long term observational archives such as OGLE (Udalski et al, 1997) and MACHO (Alcock et al, 1996). Such databases have permitted the long term optical variability to be studied, sometimes in conjunction with similar timescale X-ray databases. Two excellent examples of the science achievable from these optical archives are the results on A0538-66 (Alcock et al 2001) and AX J0051-733 (Coe et al, 2002). In the case of A0538-66 the MACHO data are shown in Figure 5.10 and clearly indicate a very regular modulation of ~ 420 d, but also evidence for activity on the much shorter 16.6d binary period (already well-known from X-ray data, Skinner 1980, 1981). Remarkably, the shorter period outbursts *only* occur during the *minima* in the 420d cycle. McGowan & Charles 2003 interpret this as being due to evolution in the circumstellar disc.

The second example of a source studied using these kinds of data is AX J0051-733. A combination of MACHO and OGLE data (Coe et al, 2002) revealed an extremely

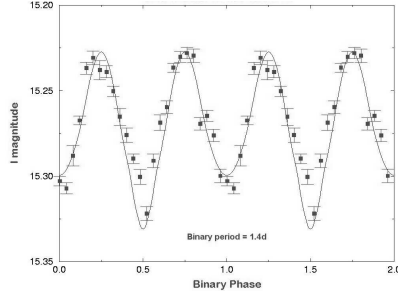


Fig. 5.11. Comparison of a representative ellipsoidal model ($i = 60^\circ$, $Q = 0.20$, $f = 0.99$, and $r_d = 0.33$) and the folded I-band data for RX J0050.7-7316. The amplitude and relative depths of the minima are roughly matched by the model. However, there are relatively large deviations, especially between phases 0.4 and 0.6 (Coe & Orosz 2000).

short modulation period of either 0.7d or double that value - see Figure 5.11. The shape of this optical modulation is driven both by tidal distortion of the envelope of the mass donor (see e.g. Avni & Bahcall 1975 and Avni 1978), and by X-ray heating effects (Orosz & Bailyn 1997). Orbital parameters such as inclination and mass ratio, may be determined from these light curves.

5.2.6 *Spectral classification of the mass donors*

The evolutionary history of Be stars in HMXBs is somewhat different to that of their isolated colleagues. The widely accepted evolutionary path is based upon conservative mass transfer developed by van den Heuvel (1983) and Verbunt & van den Heuvel (1995). The important consequence of this scenario is that wide binary orbits (200 – 600d) are produced before the final supernova explosion. Hence, any small asymmetries in the subsequent SN explosion will then produce the frequently observed wide eccentric orbits.

Of particular interest is the narrow range of spectral class revealed through blue spectroscopy of the identified counterparts (see Negueruela 1998). In contrast to the sample of isolated Be stars found in the Bright Star Catalogue, there are no known BeX objects beyond spectral class B3 - see Figure 5.12. Most commonly these have counterparts in the B0-B2 group.

The explanation offered by Van Bever and Vanbeveren (1997) for this phenomenon is that the wide orbits produced by the evolutionary models are very vulnerable to disruption during the SN explosion. This will be particularly true for the less massive objects that would make up the later spectral classes. Hence the observed distribution confirms the evolutionary models.

An excellent example of using optical spectroscopy to investigate an HMXB is the work of Covino et al (2001) on a pair of SMC objects. The blue spectrum of RX J0052-7319 (Figure 5.13) is compared to a standard star of the same spectral type, where it is clear that some of the weaker He I lines are not visible, presumably filled in by emission. All the spectral features are very shallow and broad, which is typical of a BeX counterpart and the presence of weak He II absorption places it close to

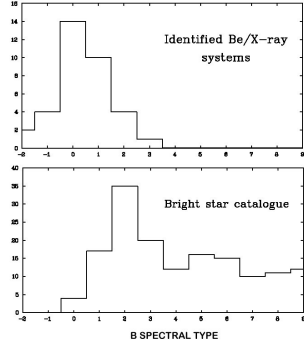


Fig. 5.12. Comparison of the spectral classes of Be stars in BeX binaries (upper) with those in isolated systems (lower). Adapted from Negueruela (1998).

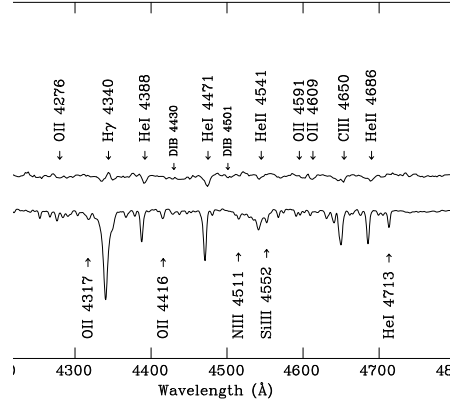


Fig. 5.13. Spectrum of the optical counterpart of RX J0052-7319 (type B0Ve) in the classification region compared to the B0V standard ν Ori (Covino et al, 2001).

B0. Furthermore, if the object is on the main sequence, the presence of weak HeII $\lambda 4200\text{\AA}$ and the condition $\text{HeII } \lambda 4541 > \text{SiIII } \lambda 4552\text{\AA}$ give a spectral type of B0Ve.

5.2.7 IR spectroscopy of HMXBs

The observations summarised in earlier sections reveal that many of the counterparts to HMXBs exhibit mass outflow to the extent of creating a circumstellar disc of material around the mass donor. Free-free and bound-free IR emission from this disc show themselves as a significant excess over the normal stellar spectrum at all wavelengths greater than the V band. This IR signature, often quantified as a J-K colour excess, is important for the following reasons:

- in confirming the identity of a Be star in the absence of optical spectral information;
- in providing an estimate of the size of the circumstellar disc (this is often directly related to the magnitude of the X-ray emission);
- through IR spectroscopy providing a channel for spectral identification in the case of objects suffering heavy optical extinction.

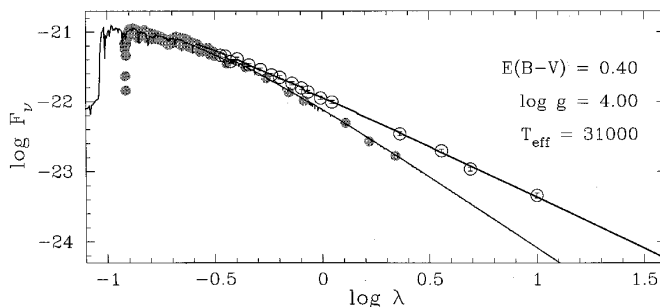


Fig. 5.14. Comparison of the optical/IR emission from X Per in two different states: with (upper curve) and without a substantial circumstellar disc Telting et al (1998).

One system that has been the subject of extensive IR observations over the years is X Per. Detailed study by Telting et al (1998) found that the density of the disc varies along with the brightness of X Per, and that in optical high states the disc in X Per is among the densest of all Be stars: $\rho_0 = (1.5 \pm 0.3) \times 10^{-10} \text{ g cm}^{-3}$. The disc density at the photosphere varies by a factor of at least 20 from optical high to low states (see Figure 5.14 for large differences taking place in the IR).

With the recent advent of IR spectroscopy on large telescopes, the possibilities of obtaining spectra despite high levels of extinction have become a reality. This is a very powerful tool for exploring previously inaccessible objects, but also directly glean information on the circumstellar environment. A good example of the strength of this new tool may be seen in Clark et al 1999 which shows the annotated IR spectra of 5 HMXBs (Figure 5.15). Just as the optical spectrum is dominated by Balmer emission, we see the same effect from the Brackett series emission in the IR. In addition, emission lines from He and metallic transitions are prominent. This approach, therefore, offers great potential for identifying and classifying the more optically obscured systems, as well as revealing the state of the circumstellar disc.

5.2.8 UV spectroscopy of HMXBs

UV spectroscopy of the mass donors in HMXBs has proved a powerful tool for understanding these systems. Since these are hot young stars they tend to be extremely UV bright. Important information about the stellar outflow may be determined from P Cygni profiles, as well as direct estimates of interstellar absorption from the 2200\AA feature which is valuable in de-coupling local and ISM extinction.

van Loon et al (2001) carried out a comprehensive study of 5 HMXBs using extensive IUE UV data. Using radiation transfer codes they derived the terminal wind velocities and sizes of the Stromgren zones created by the X-ray source from modelling the UV resonance lines. They found that these sizes were in good agreement with that expected from standard Bond-Hoyle accretion and scaled with L_X . However, the determined terminal velocities were lower than expected from single stars with the same T_{eff} - see Figure 5.16. These lower velocities could be due to the presence of the X-ray Strömngren sphere inhibiting the wind acceleration.

In addition, blue and UV spectra are essential tools for determining the precise spec-

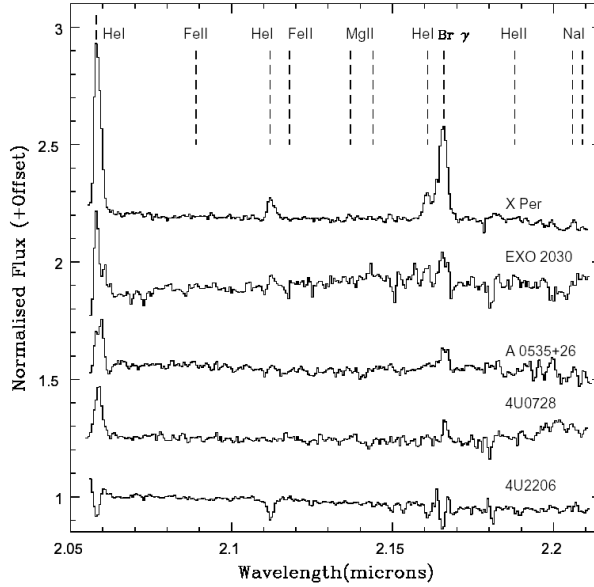


Fig. 5.15. K band spectra of BeX binaries (Clark et al, 1999). The positions of prominent H, He and metallic transitions are marked.

tral class of the mass donor, and hence information about the compact object. Clark et al 2002 used high resolution IUE UV spectra of 4U1700-37 to carry out detailed non-LTE modelling of the O type primary. Using the modelling code of Hillier & Miller 1998 which utilises radiative transfer processes in a spherical extended atmosphere, Clark et al were able to precisely define the mass donor star to be of spectral type O6.5Iaf. Combining this with binary information from eclipse monitoring, led to an accurate determination of an unusually high neutron star mass of $2.44 \pm 0.27 M_{\odot}$. This is one of the highest accurate mass determinations for a neutron star, but is not alone in pushing upwards the mass of neutron stars in HMXBs. Barziv et al 2001 have $1.87 \pm 0.20 M_{\odot}$ for the compact object mass in Vela X-1, whereas Orosz & Kuulkers 1999 find a value of $1.78 \pm 0.23 M_{\odot}$ for Cyg X-2. However, it is still conceivable that there are systematic effects at work here given how the neutron star “mass” correlates with spectral type.

5.3 LOW-MASS X-RAY BINARIES

The review by van Paradijs & McClintock (1995) remains an excellent introduction to the optical characteristics of both HMXBs and LMXBs, and Liu et al (2000, 2001) provide comprehensive catalogues of their observed properties. However, this is a field that has extended both in wavelength (with high quality UV spectroscopy available from HST/STIS, and cooled grating spectrographs allowing IR spectroscopy) and sensitivity (the advent of large telescopes such as Keck, VLT, Subaru and VLT) during the last decade. Consequently this section will focus on these later developments, and in particular on the sub-class of *X-ray transients* which

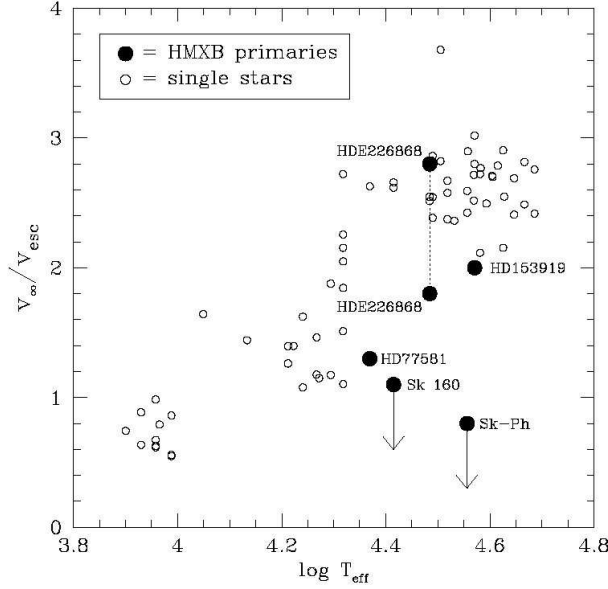


Fig. 5.16. The ratio of terminal over escape velocity for the mass donor stars in 5 HMXBs compared to isolated stars. The HMXBs have low terminal velocities for their effective temperatures van Loon et al(2001).

have allowed us to gain a far more detailed knowledge of the properties of the mass donor in LMXBs than was possible a decade ago. Additionally, gains in CCD technology now permit high time resolution photometry and spectroscopy and a consequential improvement in our understanding of luminous accretion discs.

5.3.1 Fundamental Properties

The presence of a “steady” X-ray source implies that the companion fills its Roche lobe, and so (Paczynski 1971)

$$R_2/a = 0.46(1 + q)^{-1/3} \quad (5.1)$$

where the mass ratio $q = M_X/M_2$. Combined with Kepler’s 3rd Law, then

$$\rho = 110/P_{hr}^2 \quad (5.2)$$

where ρ (in g cm^{-3}) is the mean density of the secondary. *

These stars are presumed to be on or close to the lower main sequence, then $M_2 = R_2$ and hence $M_2 = 0.11P_{hr}$ (a detailed observational analysis of the secondary stars in CVs and LMXBs can be found in Smith & Dhillon 1998). Hence short period X-ray binaries must be LMXBs, their companion stars will be faint, and the optical light will be dominated by reprocessed X-radiation from the disc (or heated face of the companion star, although this is likely substantially shielded by the disc itself;

* N.B. the Paczynski relation is only valid for $q > 1$, and there is a more accurate algorithm (Eggleton 1983) which is valid for all q .

see van Paradijs & McClintock 1994). This obliteration of the companion in “steady” LMXBs removes one of the key pieces of dynamical information about the binary. The optical spectra of LMXBs consist of hot, blue continua ($U - B$ typically -1) on which are superposed broad H, He emission lines, with velocity widths typical of the inner disc region ($\sim 500\text{--}1000 \text{ km s}^{-1}$), making accurate velocity information about the motion of the compact object difficult to obtain. Consequently accurate dynamical information about both components in LMXBs has been very difficult to acquire, yet is essential if accurate masses are to be determined (see next section). Hence, evidence on the nature of the compact object in most bright LMXBs is indirect, e.g. X-ray bursting behaviour for neutron stars (as few are X-ray pulsars) or fast variability as first seen in Cyg X-1 (and used as a possible black hole diagnostic, see chapter 4).

5.3.2 Dynamical mass measurements in X-ray novae

Progress in identifying the nature of compact objects in LMXBs requires dynamical mass measurements of the type hitherto employed on X-ray pulsars in HMXBs (see e.g. White et al 1995). Unfortunately, all that can be measured (in the case of Cyg X-1, and the other two HMXBs suspected of harbouring black holes, LMC X-1 and LMC X-3) is the mass function

$$f(M) = \frac{PK^3}{2\pi G} = \frac{M_X^3 \sin^3 i}{(M_X + M_2)^2} \quad (5.3)$$

where K is the radial velocity amplitude. With $M_2 \geq M_X$, then M_X is poorly constrained due to the wide range of uncertainty ($\sim 12\text{--}20 M_\odot$) in M_2 as a result of their unusual evolutionary history.

LMXB transients (usually referred to as *soft X-ray transients* (SXTs) or *X-ray novae* (XRN) provide ideal opportunities to study the properties of the secondary stars in great detail. Detected in outburst by X-ray all-sky monitors, they usually fade within timescales of months, after which the companion star becomes visible. The prototype of this sub-class is A0620-00, still the brightest of all XRN when it erupted in 1975, the data from which were comprehensively re-examined by Kuulkers (1998) producing the revised light curve shown in figure 5.17. Currently $\sim 25\%$ of XRN are confirmed neutron star systems (they display type I X-ray bursts), the remainder are all black-hole candidates, the highest fraction of any class of X-ray source (see e.g. Chen et al 1997). Their X-ray properties are discussed in chapter 4, and their optical/IR properties are summarised in table 5.3.2.

5.3.3 Quiescence studies of X-ray novae

In quiescence, XRN become a valuable resource for research into the nature of LMXBs. Typically their optical brightness has declined by a factor of ≥ 100 , with all known XRN having quiescent $V \sim 16\text{--}23$, which is now dominated by the companion. With large telescope optical/IR spectroscopy it is possible to determine its spectral type, period and radial velocity curve, the latter two giving $f(M)$ (equation 5.3), see table 5.3.2. These are separated into 3 sections: BHCs with cool secondaries, those with earlier spectral types and the neutron star XRN. Table 5.3.2 shows the

<i>X-ray Source</i>	<i>Optical/IR counterpart</i>	<i>b¹I</i>	<i>Outbursts</i>	<i>P</i> (hrs)	<i>Sp.</i> Type	<i>E_{B-V}</i>	<i>V</i> (quiesc)	<i>K*</i>	<i>vsini</i>	<i>K₂</i> (km s ⁻¹)	γ	<i>f(M)</i> (M _⊙)	<i>q</i> (=M _X /M ₂)	<i>i</i> (°)	<i>M_X</i> (M _⊙)	<i>M₂</i> (M _⊙)
BLACK HOLES																
LMXBs																
GRS1915+105 ¹	V1487 Aql	-0.2	1991+“on”	816	K III	~10	-	13	-	140	-3	9.5±3	12	70±2	14±4	1.2±0.2
J1859+226 ²	V406 Vul	+8.6	1999	9.2	-	0.58	23.3	-	-	570	-	7.4±1.1	-	-	>5	-
J1550-564 ³	V381 Nor	-1.8	1998, 00, 03	37.0	G8-K4IV	1.6	22	-	90±10	349	-68	6.9±0.7	-	72±5	9.6±1.2	-
J1118+480 ⁴	KV UMa	+62.3	2000	4.1	K7-M0	<0.02	19.6	-	114±4	701	-15	6.1±0.3	~20	81±2	6.8±0.4	0.25±0.15
GS2023+338 ⁵	V404 Cyg	-2.2	1938,56,89	155.3	K0IV	1	18.4	12.5	39±1	208.5	0	6.08±0.06	17±1	55±4	12±2	0.6
GX339-4 ⁶	V821 Ara	-4.3	frequent	42.1	-	1.1	~21	-	-	317 [†]	~+30	5.8±0.5	-	-	>2.0	-
GS2000+25 ⁷	QZ Vul	-3.1	1988	8.3	K5V	1.5	21.5	17	86±8	520	+19	4.97±0.10	24±10	56±15	10±4	0.5
H1705-25 ⁸	V2107 Oph	+9.1	1977	12.5	K	0.5	21.5	-	≤79	441	-54	4.86±0.13	>19	60±10	6±2	0.3
GRS1009-45 ⁹	MM Vel	+9.3	1993	6.8	K7-M0	0.2	~22	-	-	475	+41	3.17±0.12	7±1	67±3	5.2±0.6	0.7
N Mus 91 ¹⁰	GU Mus	-7.1	1991	10.4	K0-4V	0.29	20.5	16.9	106±13	421	+20	3.34±0.15	6.8±2	54 ⁺²⁰ ₋₁₅	6 ⁺⁵ ₋₂	0.8
A0620-00 ¹¹	V616 Mon	-6.5	1917,75	7.8	K5V	0.35	18.3	14.5	83±5	433	+4	2.91±0.08	15±1	37±5	10±5	0.6
J0422+32 ¹²	V518 Per	-11.9	1992	5.1	M1V	0.25	22.3	17.4	90±25	372	+11	1.19±0.02	9.0 ^{+2.2} _{-2.7}	45±2	4±1	0.3
IMXBs																
J1819.3-2525 ¹³	V4641 Sgr	-4.8	1999, 02	67.6	B9III	0.32	13.7	-	99±2	211	+107	3.13±0.13	2.31±0.08	75±2	7.1±0.3	3.1±0.3
J1655-40 ¹⁴	V1033 Sco	+2.5	1994-96	62.9	F6IV	1.2	17.2	-	88±5	228	-148	2.73±0.15	2.39±0.15	70±2	6.6±0.5	2.8±0.3
4U1543-47 ¹⁵	IL Lup	+5.4	1971,83,92,02	27.0	A2V	0.5	16.6	-	-	124	-87	0.25±0.01	3.6±0.4	21±2	9.4±1	2.5
HMXBs																
LMC X-3 ¹⁶	*1	-32.1	“steady”	40.8	B3Ve	0.06	17.2	-	130	235	+310	2.3±0.3	2.2-4.4	67±3	4-7	1-3
Cyg X-1 ¹⁷	HDE 226868	+3.1	“steady”	134.4	O9.7Iab	1.06	8.9	-	155	74.9	-1	0.244±0.005	0.4-0.8	27-67	>4.8	>11.7
LMC X-1 ¹⁸	*32	-31.5	“steady”	101.3	O8III	0.37	14.5	-	~150	68	+221	0.14±0.04	~0.5	2.5-6	8-20	-
NEUTRON STARS																
J2123-058 ¹⁹	LZ Aqr	-36.2	1998	6.0	K7V	0.12	21.8	-	121	299	-95	0.68±0.05	2.7±1.0	73±4	1.5±0.3	0.5±0.3
Cen X-4 ²⁰	V822 Cen	+23.9	1969,79	15.1	K3-5V	0.1	18.4	14.8	43±6	150	+184	0.22±0.01	5.9±1.6	43±11	1.5±1.0	0.3±0.2

References: * mostly from Wachter 1998; ¹Greiner et al 2001; ²Filippenko & Chornock 2001; Hynes et al, 2002b; Zurita et al 2002b; ³Orosz et al 2002a; ⁴Wagner et al 2001; Hynes et al 2000; Orosz 2001; Zurita et al 2002a; ⁵Casares et al 1992; Casares & Charles 1994; Shahbaz et al 1994b; ⁶Hynes et al 2003b; [†]Bowen fluorescence velocity, see section 5.3.9; ⁷Filippenko et al 1995a; Beekman et al 1996; Harlaftis et al 1996; ⁸Filippenko et al 1997; Remillard et al 1996; Martin et al 1995; Harlaftis et al 1997; ⁹della Valle et al 1997; Filippenko et al 1999; Gelino 2003; ¹⁰Orosz et al 1996; Casares et al 1997; Shahbaz et al 1997; Gelino et al 2001a; ¹¹McClintock & Remillard 1986; Orosz et al 1994; Marsh et al 1994; Shahbaz et al 1994a; Gelino et al 2001b; ¹²Filippenko et al 1995b; Beekman et al 1997; Harlaftis et al 1999; Webb et al 2000; Gelino & Harrison 2003; ¹³Orosz et al 2001; Orosz 2003; ¹⁴Orosz & Bailyn 1997; van der Hooft et al 1997, 1998; Hynes et al 1998; Shahbaz et al 1999b, 2000; Greene et al 2001; Beer & Podsiadlowski 2002; Shahbaz 2003; ¹⁵Orosz et al 2002b; ¹⁶Kuiper et al 1988; ¹⁷Herrero et al 1995; Brocksopp et al 1999; ¹⁸Hutchings et al 1983, 1987; ¹⁹Tomsick et al 2001, 2002; Hynes et al 2001a; Casares et al 2002; Shahbaz et al 2003; ²⁰McClintock & Remillard, 1990; Shahbaz et al 1993; Torres et al 2002

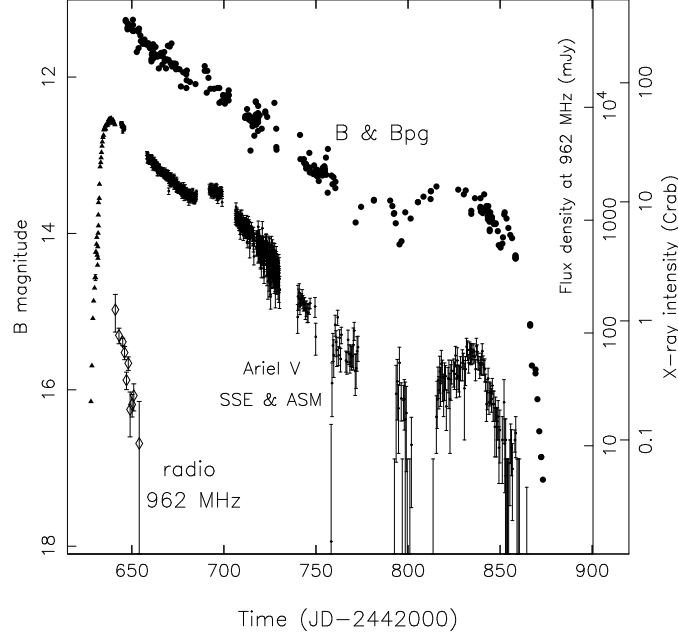


Fig. 5.17. Optical, X-ray and radio outburst light curves of the prototype XRN A0620-00 (=Nova Mon 1975) showing the typical fast rise, exponential decay on a timescale of months, adapted from Kuulkers (1998).

significance of such work, since all are LMXBs with $M_X > M_2$. N.B. $f(M)$ represents the *absolute minimum* values for M_X since we must have $i < 90^\circ$ and $M_2 > 0$.

Some dynamical information can be derived even during outburst, given spectroscopic data of sufficient resolution. Casares et al (1995) observed GRO J0422+32 during an X-ray mini-outburst and found intense Balmer and HeII λ 4686 emission modulated on what was subsequently found to be P_{orb} . Furthermore, a sharp component within the (highly complex) HeII emission profile displayed an S-wave that was likely associated with the accretion hotspot.

However, to determine M_X , additional constraints are needed in order to infer values for M_2 and i .

5.3.3.1 Rotational broadening of companion spectrum

In short period interacting binaries the secondary is constrained to corotate with the primary and must also be filling its Roche lobe (in order for mass transfer to occur). Hence R_2 is given by equation (5.1), and then (Wade and Horne, 1988)

$$v_{rot} \sin i = \frac{2\pi R_2}{P} \sin i = K_2 \times 0.46 \frac{(1+q)^{2/3}}{q} \quad (5.4)$$

from which q can be derived if v_{rot} is measured. Typically $v_{rot} \sim 40\text{--}100\text{ km s}^{-1}$, which requires high resolution and high signal-to-noise spectra of the secondary.

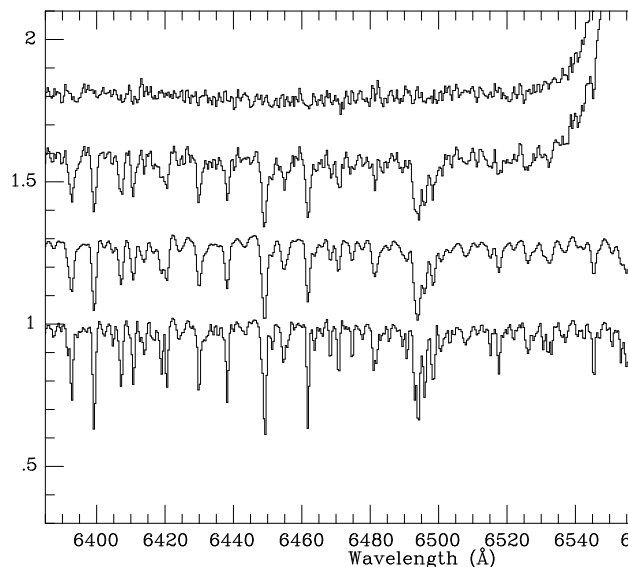


Fig. 5.18. Determining the rotational broadening in V404 Cyg. From bottom to top: the K0IV template (HR8857); the same spectrum broadened by 39 km s^{-1} ; doppler corrected sum of V404 Cyg (dominated by disc $\text{H}\alpha$ emission); residual after subtraction of the broadened template (from Casares and Charles, 1994).

The technique is demonstrated in figure 5.18 for V404 Cyg (Casares & Charles 1994) and based on Marsh et al (1994). The doppler-corrected and summed spectrum of V404 Cyg is dominated by broad $\text{H}\alpha$ emission from the disc, but the cool companion absorption features are visible and clearly broader than those of the template K0IV spectrum. The template is then broadened by different velocities (together with the effects of limb darkening), subtracted from that of V404 Cyg and the residuals χ^2 tested, giving $v_{\text{rot}} \sin i = 39 \pm 1 \text{ km s}^{-1}$ and hence $q = 16.7 \pm 1.4$. Note that small radial velocity amplitudes have also been seen in the $\text{H}\alpha$ emission (e.g. Orosz et al 1994; Soria et al 1998), but their interpretation is complex as there is a small phase offset ($\simeq 0.1$) relative to the companion (somewhat larger in GRS1009-45, see Filippenko et al 1999), and so until this is fully understood, it cannot be used to determine q .

The combination of q and $f(M)$ then yields the mass constraints (fig 5.19), and the only remaining unknown is i . To date, none of the SXTs is eclipsing (although GRO J1655-40 and XTE J2123-058 show evidence for grazing eclipses), and so it is the uncertainty in i that dominates the final mass measurement. Nevertheless there are methods by which i can be estimated.

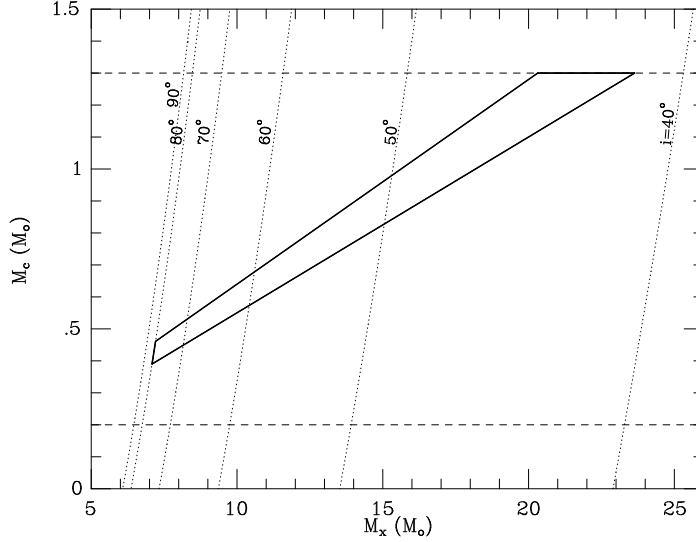


Fig. 5.19. Constraints on M_X and M_2 for a range of values of i in V404 Cyg based on the radial velocity curve ($f(M)=6.1M_\odot$ and determination of q ($=16.7$, from rotational broadening). It is the limited constraint on i (absence of eclipses) that leads to a wide range of M_X (Casares and Charles, 1994).

5.3.3.2 Ellipsoidal modulation

The secondary star in interacting binaries has a peculiarly distorted shape which gives rise to the so-called *ellipsoidal modulation* due to its varying projected area as viewed around the orbit. This leads to the classical double-humped light curve (fig 5.20), which is well defined by theory (i.e. the form of the Roche lobe) and the observed light curve depends principally on q and i . For large q values (≥ 5) the ellipsoidal modulation is largely insensitive to q and hence can provide excellent constraints on i . For full details of the light curve modelling see Tjemkes et al (1986), Orosz & Bailyn (1997) and Shahbaz et al (2003), the results from which are in table 5.3.2.

5.3.4 Mass Determinations and Limitations

To derive full XRN orbital solutions requires assuming that the quiescent secondary fills its Roche lobe (reasonable as doppler tomography of quiescent XRN reveals ongoing mass transfer; Marsh et al 1994), and that the light curve is *not* contaminated by any other emitting region. This latter assumption is questionable, since emission lines are definitely attributable to a quiescent disc, but residual X-ray heating and coronal activity on the secondary might also be present (e.g. Bildsten & Rutledge 2000). For this reason, secondary light curves are usually derived in the IR whenever possible. The disc contribution in the optical around $H\alpha$ is obtained as

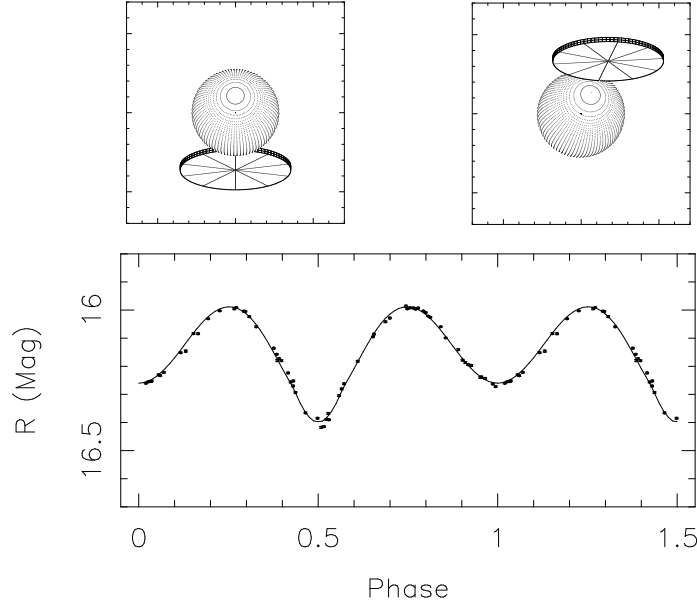


Fig. 5.20. R-band light curve of GRO J1655-40 in quiescence (van der Hooft et al 1997) together with schematics of the system orientation (Orosz & Bailyn 1997) which show the grazing eclipses required by the fits to the light curve.

a by-product of the spectral type determination, and is typically $\leq 10\%$. It should therefore be even less in the IR for a typical disc spectrum. However, the outer disc can be an IR emitter in CVs (Berriman et al 1985) and hence contaminate the light curves (Sanwal et al 1996). This is potentially significant, since a contaminating (and presumably steady) contribution will reduce the amplitude of the ellipsoidal modulation, and hence a lower i would be inferred, leading to an erroneously high mass for the compact object.

Nevertheless Shahbaz et al (1996, 1999a) showed via IR K-band spectroscopy of V404 Cyg and A0620-00 that any contamination must be small and hence the masses derived need (at most) to be reduced by only small amounts. Furthermore, in studying the non-orbital optical variability in V404 Cyg, Pavlenko et al (1996) found that (as first noted by Wagner et al 1992) the ellipsoidal modulation could be discerned underlying the substantial (short-term) flickering in the light curve. Interpreting the flickering as a completely independent component (recently verified by Hynes et al 2002a), Pavlenko et al showed that the *lower envelope* of this light curve (rather than the mean) produced an ellipsoidal light curve which, when fitted as described above, gave essentially identical results to those obtained from the IR ellipsoidal fitting, thereby providing further weight to the significance of the final mass determinations in table 5.3.2. Note that the values for Cen X-4 and XTE J2123-058 (both neutron star XRN, identified on the basis of their type I X-ray bursts) have been derived exactly by the method outlined here and yield values in excellent accord

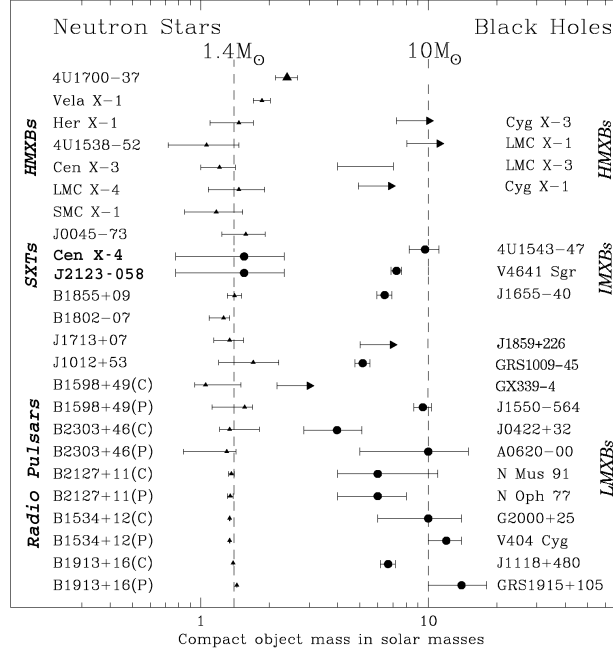


Fig. 5.21. The mass distribution of neutron stars and black holes. Note the remarkably narrow spread of NS masses, and the large factor by which the BH masses exceed the (canonical) maximum NS mass of $3.2M_{\odot}$.

with those expected for a neutron star. Table 5.3.2 contains only those systems for which a dynamical study of the companion star has been performed (all via direct detection of the spectral signature of the mass donor, except for GX339-4 - see section 5.3.9). There are a number of additional BHC (based on their X-ray and other properties) for which such studies have not yet been possible (secondary too faint or too heavily reddened), and these are listed in chapter 4.

For completeness, we have also included in table 5.3.2 the dynamically determined HMXB compact object mass determinations. In spite of an extremely accurately determined $f(M)$, there are still large and systematic uncertainties in the mass of Cyg X-1's supergiant primary HDE 226868 and the difficulty in constraining the binary inclination (it does not eclipse). This has most recently been addressed by Herrero et al (1995) whose high resolution optical spectroscopy and detailed atmospheric modelling give a mass range of 12–19 M_{\odot} for the OBI primary. With i relatively poorly constrained to 28–67 degrees, the compact object mass must be in the range 4–15 M_{\odot} . HDE 226868 has also been studied by LaSala et al (1998) and Brocksopp et al (1999) who have derived a much improved orbital ephemeris, and Bałucińska-Church et al (2000), who used this new ephemeris to study the distribution of X-ray dips as a function of orbital phase (there is a strong orbital modulation). In spite of this large uncertainty in compact object mass (a feature shared by the LMC HMXBs LMC X-1 and LMC X-3), Cyg X-1 remains a very strong BHC, and its X-ray properties are still invoked as black hole characteristics (see chapter 4).

Interestingly most of the compact object masses so far determined lie in the range 6–14 M_{\odot} , so that even the lowest value is well above the theoretical neutron star maximum mass of $\sim 3.2M_{\odot}$ (and even further from the directly measured neutron star masses of 1.35 M_{\odot} ; see Thorsett & Chakrabarty 1999 and fig 5.21). There is only one compact object mass currently in the range 2–5 M_{\odot} (the recently determined value for GRO J0422+32 by Gelino & Harrison 2003, but GRS1009-45 is close), which is curious and may be a selection effect. Certainly V518 Per and MM Vel are two of the faintest in quiescence, but it may also be possible that transient behaviour is suppressed. In such cases mass determination becomes difficult as the disc dominates the optical light, but alternative methods are now possible in certain circumstances (see section 5.3.9), or if the donor is sufficiently bright to be detectable even against the glare of the disc (GRS 1915+105, Cyg X-2).

5.3.5 *Abundance Analyses of the Mass Donors*

The absence of (significant) X-ray heating allows for detailed chemical analyses of the mass donors in the brighter of the quiescent XRN. An immediate (and unexpected) by-product of the high resolution radial velocity study of V404 Cyg was the discovery of strong LiI $\lambda 6707$ absorption (Martín et al 1992). Li is typically present in young, pre-main sequence and T Tau stars, but is destroyed by subsequent convection in late-type stars, and normal (solar) abundances are a thousand times lower. Similar Li enhancements are found in many (but not all) quiescent XRN (see Martín et al 1996), including the NS XRN Cen X-4, so this is *not* a potential BH signature.

As highly evolved objects which are extremely unlikely to have retained such high Li abundances, mechanisms have been sought that create Li within XRN, which could be important for the wider study of the galactic Li enrichment relative to the halo. Li has been seen in XRN with a wide range of P (and hence donor sizes), but their common feature is the recurrent, high L_X X-ray outbursts (CVs do *not* exhibit Li, Martín et al 1995), which led Martín et al (1994) to suggest that spallation could produce Li in large quantities close to the compact object, and might explain the 476keV γ -ray feature observed during the N Mus 1991 outburst (Sunyaev et al 1992; Chen et al 1993). Originally interpreted as the gravitationally redshifted e^-e^+ 511keV line (see also Kaiser & Hannikainen 2002), it might instead be associated with the ${}^7\text{Li}$ 478keV line. Some of this Li would be transferred to the secondary during subsequent large mass outflows. However, Bildsten & Rutledge (2000) point out that the XRN Li abundances are only slightly higher than those detected in the chromospherically active RS CVn systems and also the pre-CV binary V471 Tau. This suggests a possible link with coronal activity, although it has been argued by Lasota (2000) that this cannot account for the levels of X-ray emission seen in quiescent XRN.

More dramatic processes, and a possible link of XRN with hypernovae has resulted from the discovery by Israelian et al (1999) of substantial (factors 6 to 10) increases in the α -element abundances (O, Mg, Si, S) in very high resolution spectra of the F sub-giant donor in GRO J1655-40. Other elements (such as Fe) show entirely normal (solar) abundances, and so Israelian et al infer that the companion star was bathed in these elements which were created by explosive nucleosynthesis during

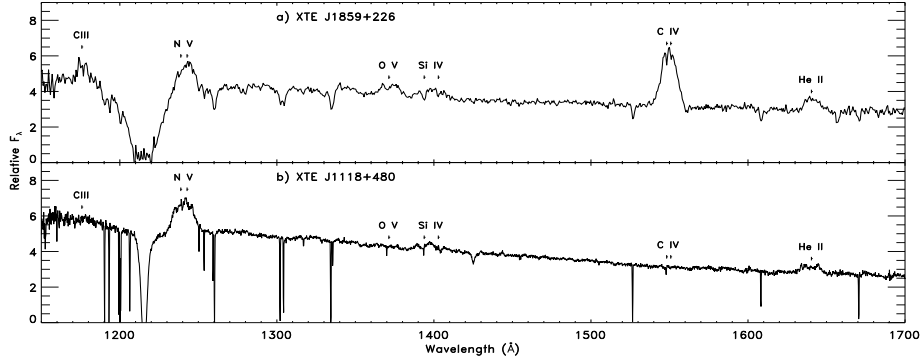


Fig. 5.22. HST/STIS UV spectra of XTE J1859+226 (upper), which shows normal line ratios (CIV more prominent than NV), whereas XTE J1118+480 (lower) has CIV and OV absent, yet NV is prominent (from Haswell et al 2002).

the supernova that formed the compact object. Interestingly, Israelian et al point out that the current BH mass estimate ($>5.5M_{\odot}$; table 5.3.2) requires a hypernova explosion in order to account for the observed abundances (see also Podsiadlowski et al 2002).

5.3.5.1 UV Spectroscopy

The evolutionary history of XRN can also be inferred from relative abundances of nuclear processed material, e.g. through UV spectroscopy. A comparison by Haswell et al (2002) of J1118+480 and J1859+226 (both observed by HST/STIS near outburst peak) revealed remarkably similar strengths of NV and SiIV, yet J1118+480 exhibited no CIV or OV (fig 5.22). This is very surprising since CIV and NV are both resonance lines of Li-like ions and therefore produced under similar physical conditions. This dramatic difference between these two short period systems implies that the mass donor in J1118+480 must have lost its outer layers, thereby exposing inner material which has been mixed with CNO-processed matter from the core (the evolution of the C/N ratio as a function of M_2 is shown in chapter 13 and Ergma & Sarna 2001). Such an interpretation requires that mass transfer began at an initial secondary mass of $\sim 1.5M_{\odot}$ and P of ≥ 12 h, but this raises interesting questions as to how the binary then evolves to its current $P = 4.1$ h (see chapter XX). However, this does support the results of Smith & Dhillon (1998) whose detailed analysis of the secondary properties in CVs shows that (up to $P \sim 7$ -8h) they are indistinguishable from main-sequence stars in detached binaries, whereas the XRN secondaries have much larger radii and are therefore evolved.

The HST spectra of J1859+226 (Hynes et al 2002b) also display a strong $\lambda 2175$ feature that allows for an accurate determination of $E(B-V)$. Combined with optical spectroscopy, Hynes et al find that the UV/optical region can be well fit by a standard, but *irradiated* disc. As the outburst progresses, the irradiated component

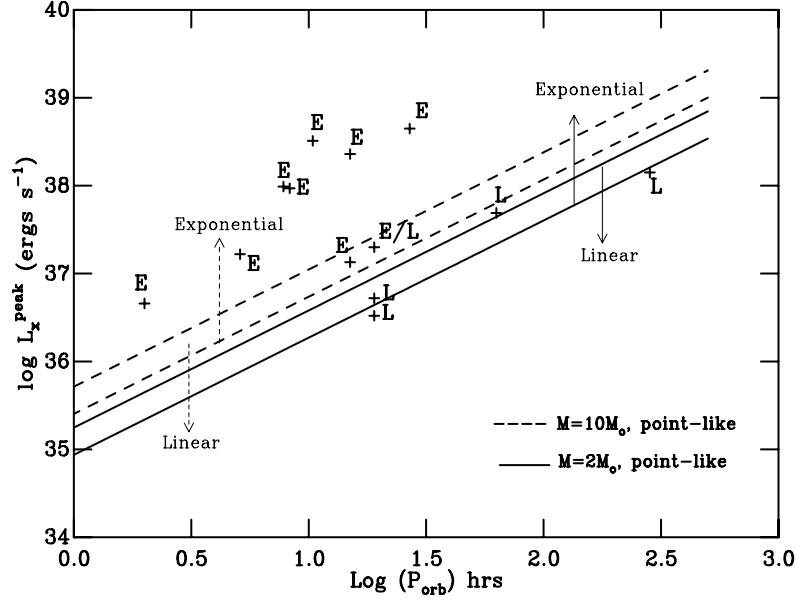


Fig. 5.23. The critical L_X needed to ionise the entire accretion disc (Shahbaz et al 1998), for total masses of 2 and $10M_\odot$ corresponding to NS and BH SXTs respectively. These L_X are a factor 2 smaller for exponential (E) decays compared to linear (L) ones, due to the difference in the disc circularisation and tidal radii. The SXTs shown are SAX J1808.4-3658, GRO J0422+32, A0620-00, GS2000+25, GS1124-68, Cen X-4, Aql X-1, 4U1543-47, GRO J1655-40 and GRO J1744-28.

declines and the implied outer disc radius reduces, implying that the system fading is a result of a *cooling* wave moving inwards (see also Lasota 2001).

5.3.6 Outburst/Decline Properties

5.3.6.1 Light curve shapes and average properties

The wide variety of X-ray light curve shapes and outburst behaviour has been reviewed by Tanaka & Shibasaki (1996), Chen et al (1997) and updated in chapter 4. But the basic shape of a fast rise and exponential decay (fig 5.17) has been interpreted as a disc instability (see Cannizzo 1998, King & Ritter 1998 and chapter 16) and is a natural consequence of an X-ray irradiated disc being maintained in a hot (viscous) state (and hence producing much longer outbursts than in dwarf novae, see King & Ritter). Furthermore, Shahbaz et al (1998) have shown that SXTs can exhibit both exponential and linear decays, the latter occurring if the SXT outburst L_X is insufficient to ionise the disc outer edge (see fig 5.23 for XRN with known P_{orb} and well-defined light curve shape).

Additionally, Shahbaz & Kuulkers (1998) [229] have shown (fig 5.24) that the optical outburst amplitude ΔV is related to P_{orb} (if $P_{orb} < 1$ day) according to:

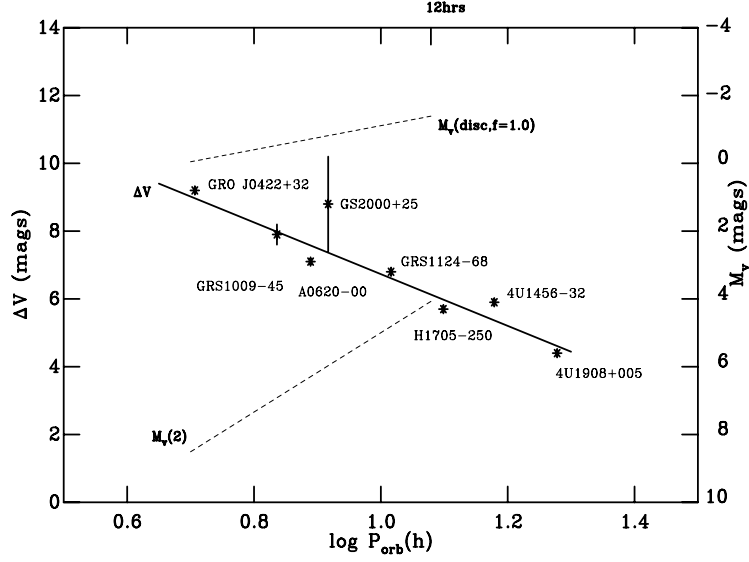


Fig. 5.24. Visual outburst amplitude of SXTs as a function of P_{orb} (Shahbaz & Kuulkers 1998). The dashed lines show the calculated disc M_V in an outbursting SXT and the donor M_V according to Warner (1995).

$$\Delta V = 14.36 - 7.63 \log P_{orb}(hrs) \quad (5.5)$$

which is essentially due to longer P_{orb} systems having larger and hence brighter mass donors (since they must be Roche-lobe filling). Hence a guide to P_{orb} can be immediately obtained once ΔV is known.

5.3.6.2 Do Superhumps Occur in LMXBs?

The high q values of XRN are also implied by the detection of *superhumps* in their optical light curves (during outburst decay; O'Donoghue & Charles 1996). As discussed in Warner (1995 and references therein), superhumps occur during *super-outbursts* of SU UMa-systems and are attributed to tidal stressing of the accretion discs in high q interacting binaries.

A wide range of models were proposed to account for this remarkable feature, but it is now widely accepted that SU UMa superhump are due to tidal energy release in an elliptical, precessing disc which occurs when the disc expands beyond its stability radius (Whitehurst & King 1991). However, this requires a high q (≥ 3) or else the stability radius is outside the tidal radius, and hence matter is simply lost from the system. With white dwarf masses typically $\leq 1M_{\odot}$ this implies very low mass secondaries and is expected to occur in short P systems (almost all SU UMa are below the period gap). Mineshige et al (1992) showed that the period excess Δ ($= (P_{SH} - P_{orb})/P_{orb}$) is related to q via

$$\Delta = \frac{3}{4} q^{-1/2} (1+q)^{-1/2} \left(\frac{R_D}{a}\right)^{3/2} \quad (5.6)$$

where R_D is the disc radius and a the orbital separation, and hence there is the potential for deriving some dynamical information from a simple measurement of the superhump Δ .

This basic model for the superhump phenomenon makes no requirement on the nature of the compact object, merely the value of q , implying that high q LMXBs, in which the compact object is now a NS or BH, should also display this effect. However, the much greater depth of the compact object potential well ($\geq 10^3$) in LMXBs implies that their intrinsic L_X exceeds that of CVs by the same factor, and hence that X-ray irradiation of the disc produces optical emission that far exceeds the *intrinsic* light of the disc, i.e. the tidal forces that produce superhumps should be swamped by irradiation. Nevertheless, observations have revealed effects related to the high q in both XRN and double-degenerate LMXBs (such as X1626-671 and X1916-053, see section 5.3.12). While the latter are confirmed (via X-ray bursts) as NS, their ultra-short P (41 and 50 mins respectively) require a degenerate, and hence very low mass donor, so that q is very high in both cases.

This potentially important effect has been explained by Haswell et al (2001) who utilised the results of disc simulations in extreme q binaries by Murray (2000). These simulations clearly demonstrated the onset of the 3:1 instability that leads to the precessing, elliptical disc (see Whitehurst & King 1991), but they also showed that the effective area of the disc is also modulated on the superhump period. And if the disc area is modulated at a given period, then so will the reprocessed light, which is the dominant factor in LMXBs. This effect is also independent of i , as observed, unlike reprocessing in the heated face of the companion. The significance of this feature in transient LMXBs where the compact object is suspected of being a black hole is that its observation can lead to an estimate of the compact object mass even while the outburst is ongoing. However, there are many “steady” LMXBs (those in bold in table 5.3) where the periodicity observed has not yet been confirmed as orbital in origin (and requires either eclipses or a radial velocity curve). Such systems are ideal targets for future application of the Bowen fluorescence mechanism (section 5.3.9).

5.3.7 *Outburst spectroscopy of GRO J1655-40*

Obtaining dynamical information during the outburst/decline phases would be extremely valuable, as the majority of quiescent SXTs are extremely faint. The superluminal transient GRO J1655-40 (see Mirabel & Rodriguez 1999) exhibited extended intervals of activity in 1994 and 1996, during which Soria et al (1998) followed the orbital behaviour of its strong, complex H α emission, but the asymmetric profile precluded its use as a dynamical tracer of the compact object. However, the broad wings of the double-peaked HeII λ 4686 emission were found to be representative of the inner disc regions, giving a radial velocity curve in anti-phase with the companion star to within $9 \pm 20^\circ$. Unfortunately, it is still difficult to use this for dynamical information as the HeII mean velocity is -182 km s^{-1} , whereas the secondary absorption lines give -142 km s^{-1} (both with very small errors). This systematic blue shift

Table 5.3. *LMXB Modulation Properties*

<i>Source</i>	Period (hrs)	Nature of modulation	X-ray type
X1820-303	0.19	X-ray	Burster, glob.cl.
4U 1850-087	0.34	UV	Burster, glob.cl.
X1626-673	0.7	opt sideband	Burster, Pulsar
X1832-330	0.73	UV	Burster, glob.cl.
X1916-053	0.83	X-ray, opt	Burster, Dipper
J1808.4-3658	2.0	pulsation RV	Burster, Pulsar, Transient
X1323-619	2.9	X-ray dip	Burster, Dipper
X1636-536	3.8	opt	Burster
X0748-676	3.8	eclipsing	Burster, Dipper, Transient
X1254-690	3.9	X-ray dip	Burster, Dipper
X1728-169	4.2	opt	
X1755-338	4.4	X-ray dip	Dipper
X1735-444	4.6	opt	Burster
J0422+32	5.1	opt RV	BH, Transient
X2129+470	5.2	opt	ADC
X1822-371	5.6	eclipsing	ADC
J2123-058	6.0	eclipsing	Burster, Transient
N Vel 93	6.9	opt RV	BH, Transient
X1658-298	7.2	X-ray dip	Burster, Dipper
A0620-00	7.8	opt RV	BH, Transient
G2000+25	8.3	opt RV	BH, Transient
A1742-289	8.4	eclipsing	Burster, Transient
X1957+115	9.3	opt	
N Mus 91	10.4	opt RV	BH, Transient
N Oph 77	12.5	opt RV	BH, Transient
Cen X-4	15.1	opt RV	Burster, Transient
X2127+119	17.1	eclipsing	Burster, ADC, glob.cl.
Aql X-1	19	opt	Burster, Transient
Sco X-1	19.2	opt	Prototype LMXB
X1624-490	21	X-ray dip	Dipper
N Sco 94	62.6	opt RV	BH, Transient
V404 Cyg	155.4	opt RV	BH, Transient
2S0921-630	216	eclipsing	ADC
Cyg X-2	235	opt RV	Burster
J1744-28	283	pulsation RV	Burster, Pulsar, Transient

adapted from Charles (2001), van Paradijs & McClintock (1995) and van Paradijs (1998)

in the disc (emission) lines suggests the presence of a substantial disc wind during X-ray high states.

Combined with one of the earliest spectral types (mid-F), the high γ -velocity suggests that GRO J1655-40 might have been formed via accretion-induced collapse of a neutron star (Brandt et al 1995). Furthermore, after its initial 1994 outburst, a subsequent optical rebrightening began ~ 6 days before the X-rays, indicating an “outside-in” outburst of the accretion disc (Orosz et al 1997). This substantial delay is due to the inner disc needing to be re-filled before accretion onto the compact object begins again, it having been evaporated by hard X-rays from the ADAF flow during quiescence (see Hameury et al 1997).

GRO J1655-40 is extremely important amongst the XRN because of its brightness in quiescence, thereby yielding high quality photometric light curves and high resolution phase-resolved spectroscopy, from which the orbital system parameters can be derived (Orosz & Bailyn 1997; but note the error analysis of van der Hooft et al 1997). The early spectral type also means that GRO J1655-40 has a low mass ratio ($q \sim 3$), and hence the ellipsoidal modulation is sensitive to both q and i (the latter being constrained by the observed grazing eclipse, see fig 5.20). The advanced evolutionary state of the secondary (which has been addressed by Kolb et al (1997), Kolb (1998) and Beer & Podsiadlowski (2002) is driving the much higher mass transfer rate, but it returns to the transient domain following temporary drops in \dot{M} .

5.3.8 Effects of Irradiation

(a) *Echo Mapping.* Many of the X-ray transients are sufficiently bright during outburst, that rapid X-ray variability provides a signature that allows “echo mapping” to be employed, which can probe the binary geometry. Although well-developed for mapping AGN structure (see e.g. Horne 1999a), its application to LMXBs requires high time resolution (\leq secs) at optical/UV wavelengths, because of the \sim seconds light-travel time across short-period LMXBs. This imposes a severe constraint on current technology, and is provided by few observatories due to the limitations of normal CCD cameras. However, HST does provide this facility, and Hynes et al (1998) obtained simultaneous X-ray (RXTE) high speed optical/UV FOS spectroscopy of GRO J1655-40 during its extended outburst, that showed the optical lagging the X-ray by ~ 10 – 20 s at times of X-ray flaring activity (see fig 5.25). With a relatively long P_{orb} (2.6d) and well-established orbital ephemeris, this optical delay can be explained entirely by reprocessing within the accretion disc and not heating of the secondary.

More recently, Kanbach et al (2001) and Hynes et al (2003a) performed a similar study (using fast ground-based photometry and HST/STIS UV spectroscopy respectively) on XTE J1118+480. While the absolute HST timing is still uncertain, these data do show the longer UV wavelengths ($\sim 2700\text{\AA}$) lagging the shorter ($\sim 1400\text{\AA}$) by about 0.25s. However, the scale of variability suggests that the bulk of this component is due to synchrotron emission, and not the accretion disc.

The long-term goal of these studies is to follow such behaviour throughout several orbital cycles, which in principle would allow the system geometry to be fully mapped. Unfortunately, this is a very difficult observational programme, particularly given that at times of X-ray outburst the binary orbital ephemeris is rarely known. But given the typical recurrence timescales of XRN of 10-50 years, such opportunities will grow in future and echo mapping could become an important technique.

(b) *Distortion of the Radial Velocity Curve.* With the X-ray variability signature clearly visible in the disc’s optical/UV emission, it is likely that the (very high) outburst L_X has a significant impact on the secondary’s atmosphere. The majority of XRN have donors that, in any case, are completely undetectable during outburst, but the small sub-group of intermediate mass donors (see table 5.3.2) are sufficiently luminous to be easily spectroscopically visible at all times. This is the case with GRO J1655-40 and the original dynamical study (Orosz & Bailyn 1997) should, ideally, have been undertaken during X-ray quiescence. But in order to obtain full

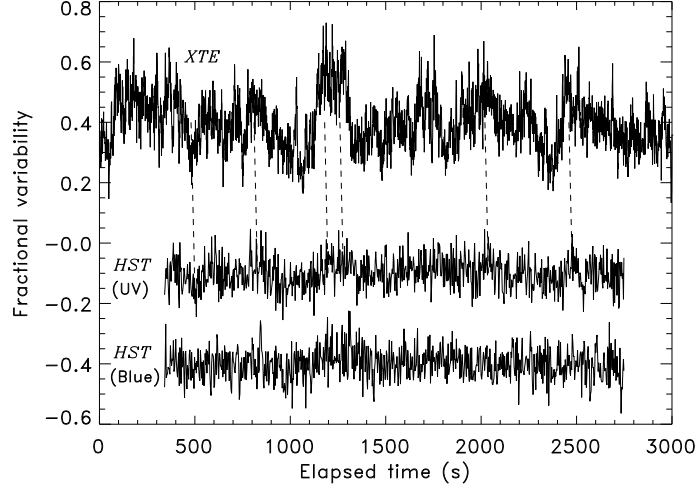


Fig. 5.25. X-ray (RXTE) and optical/UV (HST) lightcurves of GRO J1655-40 obtained in 1996 by Hynes et al (1998) which shows the ~ 10 – 20 s delay of the optical response to the X-ray flares, and are connected by dashed lines.

orbital phase coverage they did use some spectra taken during outburst. Under such circumstances, care must be taken to ensure that irradiation of the secondary has not systematically distorted the radial velocity curve.

Phillips et al (1999) tested for the presence of this effect by fitting an elliptical orbit to the Orosz & Bailyn data, which gave a highly significant $e=0.12\pm0.02$. With the ratio of incident X-ray to local stellar flux at the donor surface of ~ 7 , it is not surprising that such effects can be important. Fitting an irradiated model of the secondary with free parameters q , i and disc opening angle (which shadows the secondary’s equatorial regions) Phillips et al obtained $q=2.8$ and M_X in the range 4.1 – $6.6M_\odot$. A completely quiescent radial velocity curve was subsequently obtained by Shahbaz et al (1999, 2000) which confirmed this analysis by constraining q to the range 2.29 – 2.97 and M_X to 5.5 – $7.9M_\odot$, and updated further by Shahbaz (2003) to the values given in table 5.3.2. Hence, it is still possible (Brandt et al 1995) that the high γ -velocity of GRO J1655-40 might indicate the formation of a relatively low mass BH via accretion-induced collapse of a neutron star.

5.3.9 Spectroscopy of Luminous LMXBs

5.3.9.1 Sco X-1 and X-ray irradiation of the companion

The detailed dynamical analysis of the XRN in section 5.3.3 is only possible because of their very long quiescent intervals, during which the optical emission is dominated by the companion. This accounts for the remarkable fact that XRN account for the majority of detailed LMXB mass constraints (table 5.3.2). And since few LMXBs are X-ray pulsars, remarkably little is known of the fundamental parameters of the X-ray luminous (“steady”) LMXBs, as their companion stars are

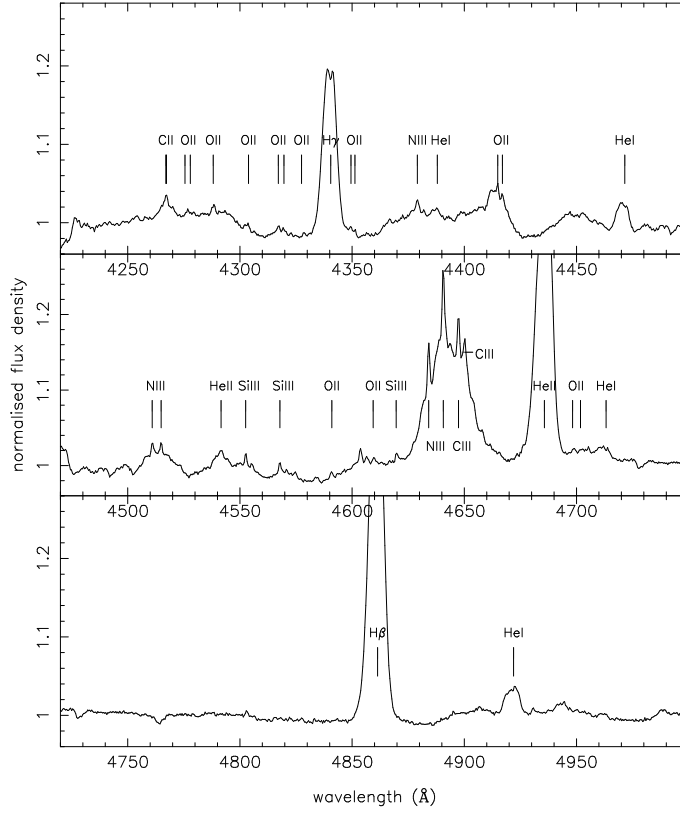


Fig. 5.26. High resolution blue spectrum of Sco X-1 (Steehgs & Casares 2002) which demonstrates the complex emission profile of the $\lambda\lambda 4640-50$ Bowen blend. Note particularly the very sharp components of NIII and CIII.

perpetually hidden from view in the glare of the X-ray illuminated accretion disc. Indeed, in spite of being the brightest LMXB in the sky (both optically and in X-rays), key parameters of Sco X-1 have only been determined quite recently. VLBA observations of its twin radio lobes give $d = 2.8 \pm 0.3$ kpc (Bradshaw et al 1999) and $i = 44 \pm 6$ degrees (Fomalont et al 2001). However, the donor has not been detected spectroscopically in either the optical (Schachter et al 1989) or IR (Bandyopadhyay et al 1997, 1999), and the optical spectrum is dominated by the X-ray irradiated disc. This situation has been transformed by Steeghs & Casares (2002) who obtained the first high resolution optical spectroscopy that revealed very sharp emission features from the Bowen $\lambda\lambda 4640-4650$ emission blend (fig 5.26).

These broad emission components produce a radial velocity curve (LaSala & Thorstensen 1985) whose phasing with respect to the lightcurve (Gottlieb et al 1975) confirms their production in the disc. However, the sharp components move in *anti-phase* to the broad emission and are therefore associated with the companion's *heated* face (fig 5.27). Note that the Bowen motion is not strictly sinusoidal, as the irradiation dominates on the inner Roche lobe that faces the X-ray source (although

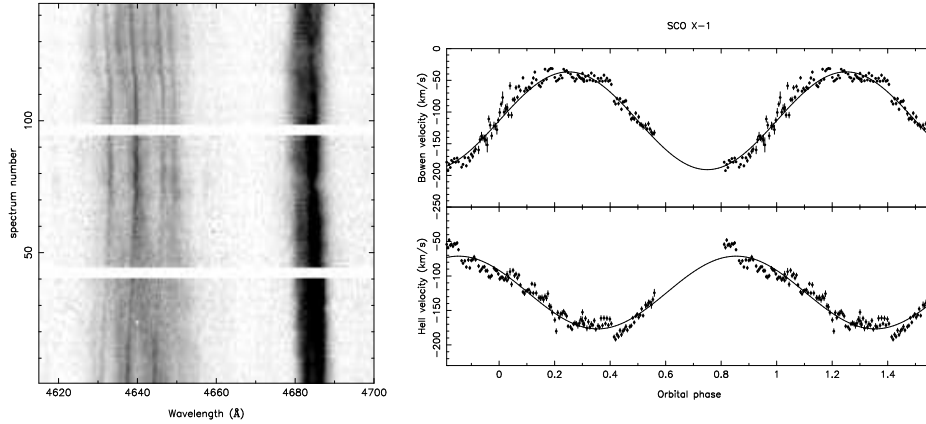


Fig. 5.27. Trailed spectrogram (*left*) and radial velocity curves (*right*) of the HeII and Bowen emission from Sco X-1 (Steehgs & Casares 2002).

there will also be some disc shadowing which will ameliorate this), and hence only the limit $K_2 > 77 \text{ km s}^{-1}$ is obtained. However, doppler tomography (see Marsh 2001 for a detailed review of this technique) of Sco X-1 with these data (fig 5.28) shows strong emission from the secondary and indicates $K_2 > 87 \text{ km s}^{-1}$. There is a slight offset with the anti-phased HeII emission ($\Delta\phi \simeq 0.1$; likely due to hot spot contamination as in CVs, see Warner 1995), but the amplitude implies $K_1 < 53 \text{ km s}^{-1}$. The doppler tomograms show that there is a HeII component on the secondary as well (but not HeI or Balmer emission, these arise completely on the disc), and this distorts the disc radial velocity curve. Searching only for the symmetric component gives $K_1 \simeq 40 \text{ km s}^{-1}$, and hence $q > 2.2$. However, Steeghs & Casares argue that the likely offset of the heated face combined with the radio-determined i yield $M_2 \sim 0.4 M_\odot$ if the neutron star has a canonical $1.4 M_\odot$. This requires an evolved secondary and hence $\dot{M} \sim 8 \times 10^{-10} M_\odot \text{ y}^{-1}$ (King et al 1996), which gives a disc $T > 6500 \text{ K}$ which is stable.

5.3.9.2 GX339-4 and XRN in outburst

This powerful new technique has already been applied to the (almost) steady LMXB BHC GX339-4 (Hynes et al 2003b). First proposed as a BHC (Samimi et al 1979) based on its Cyg X-1-like X-ray fast variability, GX339-4 moves regularly through high, low and “off” states (ref) on timescales of a year or two. Associated with these, the optical counterpart (V821 Ara) varies between $V < 15$ at peak to > 20 at minimum. Yet even at its faintest, there has been no detection of the (presumed) cool mass donor (Shahbaz et al 2001). Consequently, even P_{orb} has been ill-constrained, and so the return to an X-ray bright phase in mid-2002 provided an opportunity to apply the Bowen fluorescence technique.

The Bowen blend is indeed strong when the source is X-ray bright, and smoothly moving sharp features were detected which suggest $P = 1.76 \text{ d}$, compared to the (non-confirmed) 14.8h period of a decade earlier (Callanan et al 1992; see also Cowley et al 2002). The resulting K_2 velocity leads to the $f(M)$ given in table 5.3.2, finally

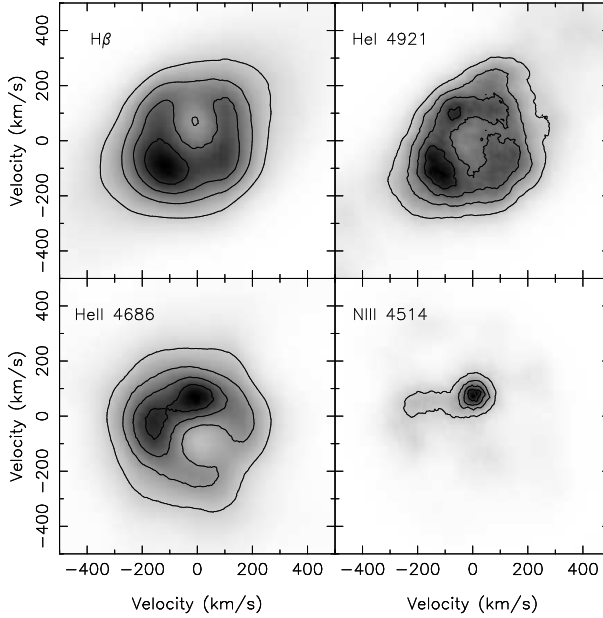


Fig. 5.28. Doppler tomograms of Sco X-1 (Steehgs & Casares 2002) where the origin is the binary centre of mass. Note the strong NIII emission located on the companion, whereas the other emission lines' ring-like structure is typical of accretion discs (although HeII also has a component on the companion).

confirming its BHC status. What is curious in this case is the fact that the sharp features are not always visible (Hynes et al 2003b), suggesting that there are significant intervals during which the face of the donor is effectively shielded from direct illumination. This could arise if the disc is either warped or is elliptical and precesses in a way that it approaches the donor (refs). Nevertheless, these results demonstrate the potential power of this technique and we anticipate substantial progress in the coming decade in determining, for the first time, the dynamical properties of the luminous LMXBs.

5.3.10 Orbital light curves and tomography of LMXBs

5.3.10.1 XTE J2123-058

The 1998 NS XRN J2123-058 is an ideal system with which to demonstrate the range of LMXB optical light curves. It has a relatively short (6h) period and orbital light curves were obtained from outburst peak through decline and into quiescence by Zurita et al (2000); see also Soria et al 1999). The high i produces a spectacular modulation that evolves from triangular to double-humped (fig 5.29) as the relative contributions of the disc, X-ray heated companion and ellipsoidal components change during the decline. These exquisite light-curves were modelled by Zurita et al (see also the re-analysis by Shahbaz et al 2003) to constrain i to be $73 \pm 4^\circ$. J2123-058 also produced a value of $\xi = B_0 + 2.5 \log F_X (\mu Jy) = 21.9$, which compares remarkably well with the canonical value for LMXB X-ray heating of 21.8 ± 1 from

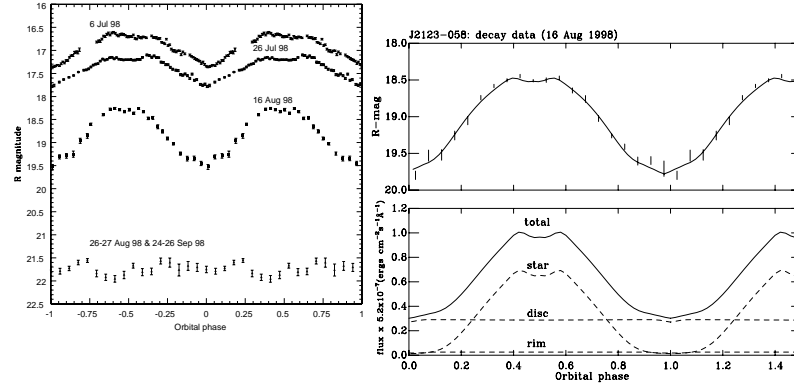


Fig. 5.29. *Left*: Orbital light curves of J2123-058 (folded on $P=6\text{h}$) from close to outburst peak (July 1998) through to quiescence several months later, showing the dramatic lightcurve evolution as L_X declines (Zurita et al 2000). *Right*: Model fit to the August decay data with the individual model components plotted below (Shahbaz et al 2003).

van Paradijs & McClintock (1994). The observation of an X-ray burst also requires the neutron star to be directly visible, and hence provides a tight constraint on the disc flare angle ($\alpha < 90^\circ$).

In addition to the outburst light curves of J2123-058, time-resolved spectroscopy (Hynes et al 2001a) through two orbital cycles permitted the application of doppler tomography in order to provide an *image* of the accretion disc, but with surprising results. Multiple S-waves are easily visible in HeII line profiles, but the doppler maps (fig 5.30) show this to be located in the lower left region (on the *opposite* side of the NS from the companion), and hence definitely *not* the donor's heated face.

Combined with transient $\text{H}\alpha$ absorption between orbital phases 0.35-0.55, Hynes et al interpret J2123-058 as the NS analog of the SW Sex phenomenon (a sub-class of CVs, see Hellier 2000). While other LMXBs, both transient (e.g. J0422+32, Casares et al 1995) and steady (e.g. X1822-371, Harlaftis et al 1997; Casares et al 2003) display their main emission at the stream-disc impact region, there are now several LMXBs with similar properties to J2123-058 (see fig 5.31). While this region of the doppler tomogram can be a result of stream overflow and subsequent re-impact on the disc (Shafter et al 1988), it requires a strongly flared disc in order to prevent the overflowing stream producing absorption at *all* phases, and this is already very tightly constrained by the light curve models described above. A more likely explanation is to invoke the *magnetic propellor* model of AE Aqr (Eracleous & Horne 1996; Horne 1999b) which involves a strong magnetic field anchored to a rapidly spinning white dwarf which accelerates matter out of the system and into a region beyond the compact object where the streams collide (fig 5.30c). However, J2123-058 involves a rapidly spinning neutron star ($P_{\text{spin}} \sim 4\text{ms}$; Tomsick et al 1999 [252]) and would present far too small an area to be effective, and so Hynes et al suggest that this process could still be occurring but with a magnetic field anchored in the disc.

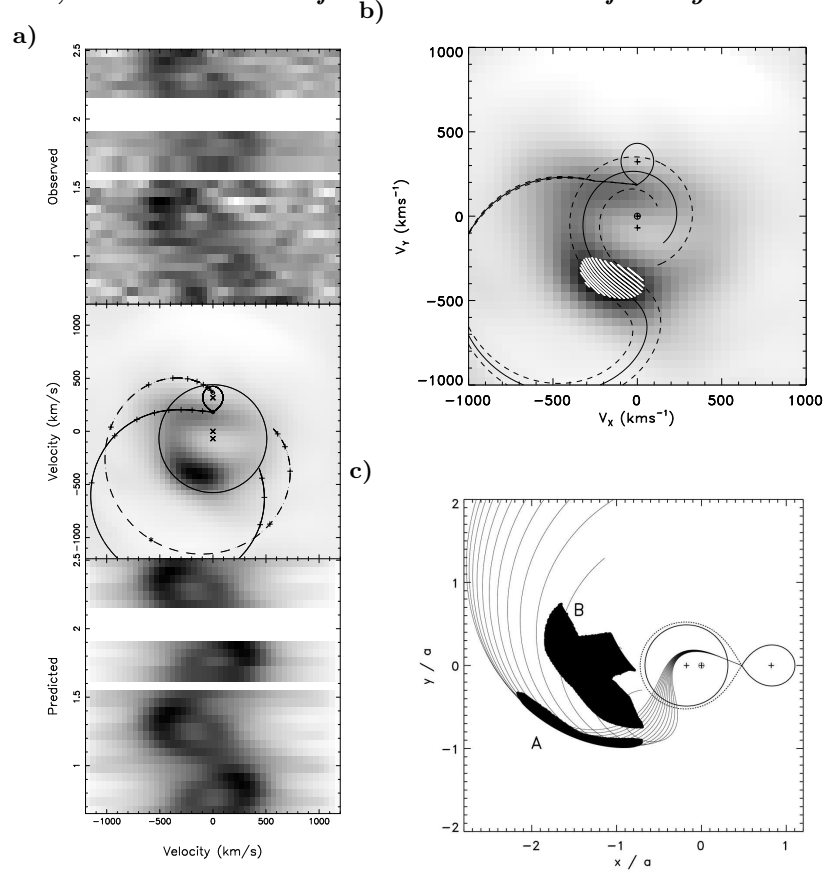


Fig. 5.30. Doppler tomography of J2123-058 during outburst (Hynes et al 2001a). a) (from top) actual data, tomogram, reconstruction. In the centre panel, the solid line is the ballistic stream trajectory, the dashed line the Keplerian velocity at the stream position and the large circle is the Keplerian velocity at the disc edge. b) Comparison between magnetic propeller trajectories and the tomogram. c) Spatial plot corresponding to (b). Points in region A produce emission with kinematics corresponding to the tomogram's white hatched region, whereas those in B produce absorption with the $H\alpha$ phasing and velocities.

5.3.10.2 Millisecond pulsar transients

Whilst the discovery of kHz QPOs in LMXBs (see chapter 2) finally demonstrated that high L_X LMXBs could indeed spin up their neutron stars to very high rates (and hence are the ancestors of radio millisecond pulsars, MSPs), it was not until 1998 that RXTE discovered the first X-ray MSP, J1808.4-3658, with $P_{spin}=2.49\text{ms}$ (Wijnands & van der Klis 1998). X-ray bursts were also seen by SAX (in't Zand et al 1998) and this fast LMXB pulsar is in a 121min orbit about a very low mass ($<0.1M_\odot$) secondary (Chakrabarty & Morgan 1998). This short-lived transient (only tens of days) peaked at $V\sim 16.6$ (Roche et al 1998), but was below $V\sim 20$ only 6 weeks later (Giles et al 1999). However, Giles et al did detect a $\Delta V \sim 0.1$ modulation on

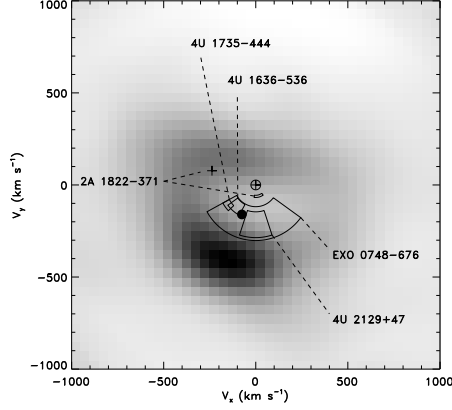


Fig. 5.31. Comparison of J2123-058's tomogram with other systems. Boxes represent uncertainties in velocity semi-amplitude and phasing. The large point is the best fit semi-amplitude and phase for J2123-058 (Hynes et al 2001b).

P_{orb} which was anti-phased with the pulsar and hence dominated by the heated face of the cool donor. Even in quiescence at $V \sim 21$, Homer et al (2001a) found a similar, sinusoidal modulation still present, which was due to the heated face, and *not* the double-humped ellipsoidal light curve seen in XRN, i.e. the secondary is *not* detectable. This can be explained by the fact that J1808.4-3658 has $F_X/F_{opt} \sim 10$ in quiescence, compared to a more typical ~ 1000 in outburst i.e. the quiescent source is still bright optically, which means that the Homer et al light curve is due to a combination of the remnant (irradiated) disc and the heated face of the donor.

Furthermore Bildsten & Chakrabarty (2001) have determined that the donor has $M_2 = 0.05 M_\odot$ and $R_2 = 0.13 R_\odot$ in order to fill its Roche lobe, and hence it must be heated by the NS (see also Burderi et al 2003), confirming that J1808.4-3658 is the progenitor of an MSP binary. The low average \dot{M} of $\sim 10^{-11} M_\odot y^{-1}$ implies that such systems can be extremely long-lived and may still be present as e.g. low L_X sources in globular clusters (as seen in 47 Tuc, see chapter 8). This class of object is extremely important as a test-bed for understanding the magnetic properties of neutron stars (Bhattacharya 2002), and will be enhanced with the extremely recent discovery by RXTE of 4 more LMXB MSPs (Markwardt et al 2002; Galloway et al 2002; Bildsten 2002; Markwardt et al 2003; Kirsch & Kendziorra 2003), all with $P_{spin} \sim 2-5$ ms.

5.3.11 Infrared spectroscopy of LMXBs

It is an unavoidable consequence of the galactic distribution of LMXBs (White & van Paradijs 1996) in which half of all LMXBs are within 20 degrees of the Galactic Centre, that the majority of these are heavily obscured in the optical and hence are accessible only in the IR (since the V/K extinction ratio is ~ 10). The most luminous of these form a sub-group known as the ‘‘Galactic Bulge Sources’’ (or GBS) which lie within a strip of $l = \pm 15^\circ$, $b = \pm 2^\circ$ about the Galactic Centre.

Several of the GBS exhibit QPOs, but rarely X-ray bursts (see chapter 3), and no clearly defined P_{orb} , hence their nature as LMXBs or HMXBs was unclear in many cases. Consequently, the accurate X-ray locations for the GBS were surveyed by Naylor, Charles & Longmore (1991) with the first generation of IR arrays. While the technology has improved over the last decade, IR spectroscopy is still limited to much brighter sources than in the optical, and so much remains to be done. Here we discuss the advances made on particular sources (e.g. Bandyopadhyay et al 1997, 1999), key properties of which are in table 5.4 together with details of other highly obscured LMXBs (apart from Sco X-1 and Cyg X-2 which are included for reference):

- GX1+4 (X1728-247) is unusual in being in a region of low reddening, where the X-ray source is coincident with a bright ($K=8.1$) M6III star at $d \sim 3-6$ kpc and hence $L_X \sim 10^{37} \text{ erg s}^{-1}$ (Chakrabarty & Roche 1997). A_V is steady (at 5.0 ± 0.6), but the X-ray column is variable, implying the presence of a wind. Its $H\alpha$ emission is not uncommon for such an object, and the identification was only secure when the $H\alpha$ flux was found to be pulsing with the same period (114s) as in X-rays (Jablonski et al 1997). While GX1+4 was, for 25 years, the brightest hard X-ray source in the Galactic Centre region (and the pulsar was spinning up), it turned “off” in the 1980s and is now on at a low level (and spinning down). Most HMXBs display an orbital modulation superposed on the pulsar’s long-term \dot{P} trend, but not GX1+4. There have been suggestions of a $\sim 304\text{d}$ variation in the accretion torque history (Cutler et al 1986) and spin-down rate (Pereira et al 1999), but there is no correlation with the X-ray flux and so these claims require confirmation. Assuming a NS mass of $1.4M_\odot$ and requiring the M6III to fill its Roche lobe implies that $P \geq 100\text{d}$.
GX1+4 is of interest as the *only* NS symbiotic system (but note 4U1700+24, Masetti et al 2002, which may be similar, although much less luminous), and hence a potential progenitor of very wide ($P \gg 10\text{d}$) radio pulsar binaries. These must have been very wide LMXBs and hence required K or M giant donors. Such rare systems (with a high \dot{M}) would appear just like a symbiotic.
- GX13+1 was identified with a $K \sim 12$ star by Naylor et al (1991) on the basis of its variability and strong $\text{Br}\gamma$ emission (fig 5.32). More importantly the spectrum also shows CO absorption bands typical of cool (K–M) stars, and the presence of ^{13}CO indicates that it is evolved. At $d \sim 9\text{kpc}$ and $E(B-V)=5.7$, then $M_K=-4.6$ and so it must be $\sim K2-M5\text{III}$. Possible periodicities in the range 13–20d have been suggested (Garcia et al 1992; Bandyopadhyay et al 2002) which would be consistent with such a classification, but further advances in understanding GX13+1 require an IR radial velocity study, which is now feasible, although observationally challenging.
- GX17+2 is a bright Z source which also bursts (and is hence a NS). It benefits from an accurate radio location (Hjellming 1978) which aligns with NP Ser, a $V \sim 17$, completely normal G star. This conundrum was settled by an HST/NICMOS image which revealed that NP Ser is actually outside the radio error circle (by 0.7 arcsecs), while two much fainter ($H \sim 20, 21$) stars are consistent with the radio location (Deutsch et al 1999). Keck observations (Callanan et al 2002), however, reveal a $K=15$ star at that position, $\sim 3.5-4$ mags brighter than the NICMOS stars! Furthermore, K-band monitoring by Bandyopadhyay et al (2002) shows that this object displays large amplitude variability once

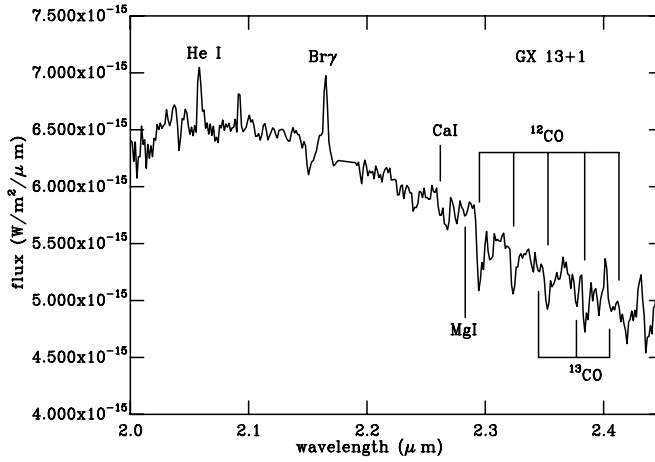


Fig. 5.32. K-band spectrum of GX13+1 (Bandyopadhyay et al 1999) showing strong He I and Br γ emission, together with CO absorption bands. Note the presence of ^{13}CO which indicates it is both cool and evolved.

corrections are made for (the unresolved) NP Ser. What is remarkable about GX17+2 is that (according to RXTE/ASM monitoring) the X-ray flux level is extremely high *and* steady, in spite of the huge IR fluctuations.

- the two SXTs, X1608-522 and X1630-47, are unusual in that they both have semi-regular outbursts on timescales of ~ 600 days (Augusteijn et al 2001; Wachter et al 2002; and references therein). They both suffer from extinction, so their optical counterparts are faint, even in outburst, but both have now been observed in the IR, with X1608-522 recently revealing a 0.54d (single peak, i.e. X-ray heated) modulation during an extended low X-ray intensity state following an outburst. Such states are compared with Z Cam “standstills” which are seen in CVs and GX339-4 (Kong et al 2002), and have also been seen in Aql X-1, another frequently outbursting, neutron star SXT.

5.3.12 Long Periods and Disc Structure in High Inclination LMXBs

The first X-ray dipper discovered, X1916-053 (Walter et al 1982), produced one of the first orbital periods of any LMXB. With type I X-ray bursts indicating the presence of a neutron star, and the ultra-short P_{orb} of 50 mins implying that the mass donor was a $\sim 0.1M_{\odot}$ degenerate dwarf, then $q \sim 15$ and hence it should also be susceptible to the SU UMa-type disc precession (section 5.3.6.2). Indeed an X-ray quasi-periodicity of ~ 199 d had already been suggested (Smale & Lochner 1992).

In spite of its faintness ($B \sim 21$; due to a combination of reddening and the low-mass donor) and crowding, an optical analogue of the X-ray dip period was found, but remarkably it was 1% longer (3027.6s versus 3000.6s)! Both periods are now precisely known and the difference is highly significant (Callanan et al 1995; Chou et al 2001; Homer et al 2001b), but debate continues as to which is orbital. Classical SU UMa-type behaviour would imply it is the X-ray, and precession induces the slightly longer optical modulation. However, unlike in SU UMa systems (where the

Table 5.4. *LMXB IR Properties*

<i>Source</i>	b^{II}	K	P (d)	IR Spectrum		Notes
				<i>emission</i>	<i>absorption</i>	
Cir X-1 ^{1,2}	0	9–12	16.54	Br γ , HeI, II	-	Super L_{Edd} , highly eccentric orbit
X1630-47 ³	+0.3	16.1	-	-	-	~ 600 -690 ^d recurrent BH transient
GX1+4 ^{4,5}	+4.8	8	~ 300	Br γ	M6III	symbiotic, X-ray pulsar (114s)
<i>Z-sources:</i>						
Sco X-1 ^{4,6}	+24	11.9	0.79	Br γ , HeI, II	-	“steady” prototype LMXB
GX340+0 ⁷	-0.1	17.3	-	-	-	luminous bulge source
Sco X-2 ⁶	+2.7	14.6	0.93/14.9	Br γ , HeI	-	“
GX5-1 ^{8,9}	-1.0	13.5	-	Br γ , HeI	-	“
GX17+2 ¹⁰⁻¹²	+1.3	14.9–18.5	~ 20	-	-	not NP Ser
Cyg X-2 ⁷	-11.3	13.3	9.8	-	A9III	IMXB
<i>atolls:</i>						
X1608-522 ^{7,13}	-0.9	16.5	0.54	-	-	NS transient
GX9+9 ⁷	+9.0	16.0	0.17	-	-	v short period
GX3+1 ¹⁴	+0.8	15.1	-	-	-	candidate ID
GX9+1 ¹⁴	+1.1	16.2	-	-	-	candidate ID
GX13+1 ^{4,6,12,15}	+0.1	11.9-12.3	~ 25 d	Br γ , HeI	CaI, MgI, ¹² CO, ¹³ CO	(see fig 5.32)

¹Johnston et al 1999; ²Clark et al 2003; ³Augusteijn et al 2001; ⁴Bandyopadhyay et al 1997;⁵Chakrabarty & Roche 1997; ⁶Bandyopadhyay et al 1999; ⁷Wachter 1998; ⁸Jonker et al 2000;⁹Bandyopadhyay et al 2003; ¹⁰Deutsch et al 1999; ¹¹Callanan et al 2002; ¹²Bandyopadhyay et al 2002; ¹³Wachter et al 2002; ¹⁴Naylor et al 1991; ¹⁵Charles & Naylor 1992

superhump period actually drifts during the ~ 2 -week superoutburst), the optical period in X1916-053 was extremely stable, suggesting that it might be the orbital period. Other models have also been invoked (e.g. a triple system, Grindlay et al 1988, Grindlay 1989).

Furthermore, detailed X-ray and optical light-curves (fig 5.33; see Homer et al 2001b; Chou et al 2001) reveal that the morphology evolves dramatically over several days, on a timescale similar (but not necessarily equal) to the X-ray-optical beat period (fig 5.33). The X-ray dipping is known to be due to azimuthal structure in the disc edge (e.g. around the stream-disc impact region) viewed at an appropriately high i (Parmar & White 1988). Any variation in this structure, or in the angle it presents relative to our line of sight, would cause the observed light curve to change. This has led to speculation that the disc in X1916-053 not only precesses but is warped, an effect expected due to X-ray irradiation (Wijers & Pringle 1999; Ogilvie & Dubus 2001). This is presumably similar to the 35d on-off cycle in Her X-1, where the tilted disc precesses relative to the observer (see e.g. Schandl & Meyer 1994). This cycle is not precise, it has some “jitter”, as is also seen in the precession of SS433 (Margon 1984).

Such a light curve modulation can also be explained by invoking a triple system

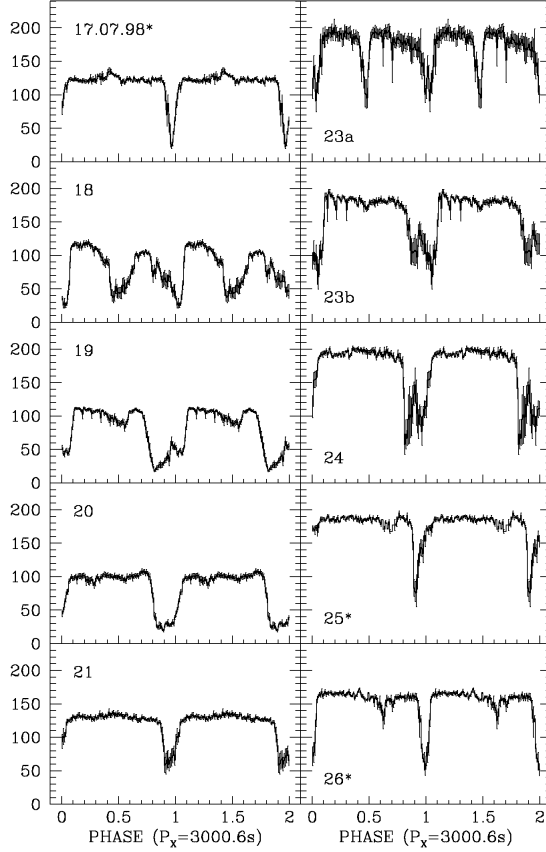


Fig. 5.33. RXTE PCA X-ray light curves of X1916-053 folded on the X-ray period of 3000.6s, in which the dipping structure clearly evolves on a timescale of days, eventually repeating (adapted from Homer et al 2001b).

(producing dips predominantly when the mass transfer rate is enhanced), which would have to be formed in a globular cluster core which has subsequently evaporated (Grindlay et al 1988). A further problem is the stability of the triple given the observed periodicities, and this model is now deemed unlikely. The effects observed are far closer to those expected from the precessing disc model related to the well-established high q . Initially the stability of the optical period was considered a difficulty, but since the mass transfer in this LMXB is basically steady (unlike in SU UMa systems) it is possible that the instability will also stay fixed at a single period, i.e. X1916-053 is a *permanent superhumper*. An alternative is to consider X1916-053 as a *negative superhumper* in which the optical period is indeed orbital, and the X-rays are now the superhump. While this is seen in a number of CVs (see e.g. Patterson 1999) the effect is not well understood (Retter et al 2002).

With its short P_{orb} and accessible (\sim days) light curve evolution, X1916-053 is an ideal system in which to study accretion disc edge structure and how it might be

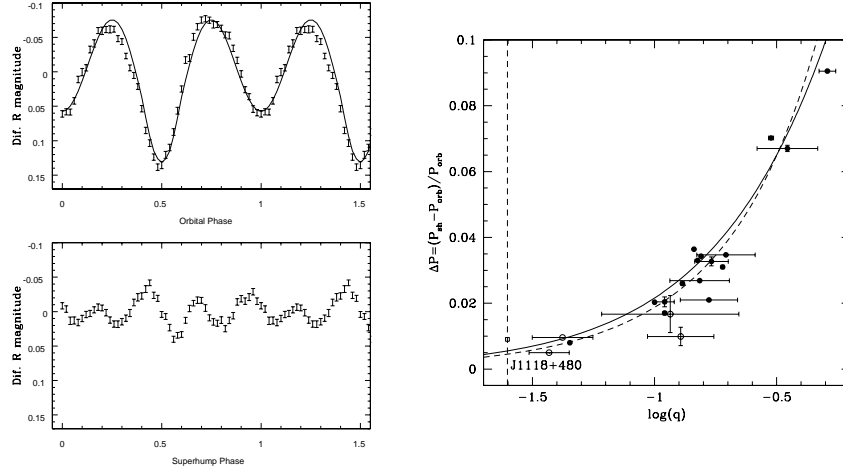


Fig. 5.34. *Left:* Detrended lightcurve (upper) of J1118+480 folded on $P_{orb}=4.078h$, together with an ($i=75^\circ$ and $q=25$) ellipsoidal model, with residuals plotted below after folding on $P_{sup}=4.092$ hours. *Right:* Combined results on LMXBs (J1118+480, X1916-053) and CVs (Patterson 2001) that display superhumps, where Δ is plotted against q . Models are plotted as solid (Patterson) and dashed (Osaki 1985 [199]) curves, but should not be valid below $q = 0.025$ (Zurita et al 2002a).

influenced by irradiation-driven warping. Such results are likely to have application well beyond this immediate field. Possibly similar behaviour has been reported in the BHC X1957+11 (Hakala et al 1999) and the system MS1603+2600 (Hakala et al 1998), the latter at high latitude and the nature of the compact object is still controversial (see e.g. Mukai et al 2001).

5.3.12.1 The halo transient, XTE J1118+480

This topic has been taken even further with extensive observations of the SXT J1118+480 (Remillard et al 2000). With its low extinction and relative proximity ($\sim 1kpc$) the late decline phase was monitored in unprecedented detail (Zurita et al 2002a). As expected once the disc contribution faded, the ellipsoidal modulation became visible (figure 5.34). However, the accretion disc component was still very significant ($\sim 50\text{--}70\%$), and temporal analysis revealed that, in addition to the ellipsoidal variation (which appears to peak at $P_{orb}/2$), there is a further modulation at a slightly longer period (visible as a distorting “wave” in the nightly light curves). Subtracting a theoretical ellipsoidal fit from the data leaves this unusually structured modulation, an effect that continues well past the original outburst (as also now seen in CVs, e.g. Patterson 1995). More surprisingly here, the period excess is extremely small, at only $\Delta \sim 1\%$.

However, such a small Δ implies (equation (5.6)) that q must be extremely high (~ 40), and hence this interpretation must be treated with great caution (fig 5.34).

At such extreme q values the classical 3:1 resonance would be replaced by the 2:1 resonance (Whitehurst & King 1991).

5.3.13 Special Cases

In this final section we discuss several high profile sources whose classification as either HMXB, LMXB or even binary is still a subject of controversy, mostly due to the absence of any direct signature of the mass donor. However, in 3 of these cases there is now circumstantial evidence that the secondaries are quite massive, but the very high implied \dot{M} gives them properties akin to LMXBs, so they transcend a simple classification.

5.3.13.1 SS433: the link with ULXs?

SS433 is the original source for studying the detailed physical processes involving relativistic jets on a galactic scale, and is still the only continuously emitting galactic micro-quasar (see chapter 9). The key feature of SS433 is its 160d precessing jet, observed for several decades (in optical, IR and X-ray) as periodic emission-line shifts which can be fitted to high precision by the *Kinematic Model* (see Margon 1984 for details and a full historical review). However, in spite of more than 20 years of detailed study, remarkably little is known about the fundamental system properties of SS433. This is a consequence of two factors: (i) the enormously powerful and broad, stationary and moving emission lines (which first brought it to attention) obliterate any spectral features of the companion; (ii) the high extinction which has severely biased most optical spectroscopy towards the red (which Goranskii et al 1998 show is in any case dominated by an erratically varying component) and hence away from where intrinsic spectral features of a massive donor might be observed. The properties of the microquasars, such as SS433 and GRS1915+105, are of great importance in furthering our understanding and interpretation of the ultra-luminous (ULX) sources in nearby galaxies (see chapters 9, 12 and 13). While SS433 appears to us as an extremely low L_X ($\sim 10^{36} \text{erg s}^{-1}$) source compared to GRS1915+105 (which peaks at $\sim 10^{39} \text{erg s}^{-1}$, and possibly up to a hundred times greater than this, once appropriate correction for extinction has been made, e.g. Greiner et al 1998), it is possible that the high i and extremely high \dot{M} of SS433 are preventing us from viewing its intrinsic L_X . In any case the observed L_X is far exceeded by the jet power, as is true in pulsar wind nebulae, but not in the other microquasars (Safi-Harb 2003).

Nevertheless, the orbital period is known (13d) and it is eclipsing in optical and X-ray light curves, but with no signature of the mass donor there exists no constraint on the dynamical masses comparable to those of the XRN described earlier. Indeed, there are published “determinations” of the SS433 compact object mass ranging from $0.8M_\odot$ (d’Odorico et al 1991) to $62M_\odot$ (Antokhina & Cherepashchuk 1985)! These are all based on radial velocity curves of the HeII emission line, of which the most detailed study is that of Fabrika & Bychkova (1990), who used ~ 4 yrs of 6m data taken around $\Psi \sim 0$ (which gives the lowest scatter in their radial velocity curve), when the disc normal was closest to our line of sight. Assuming $e=0$ they obtain $f(M) \simeq 8M_\odot$, which implies a $10M_\odot$ donor for a NS compact object, or $15M_\odot$ for a

$6M_{\odot}$ BH (and which would also better explain the extremely high $\dot{M} \sim 10^{-4} M_{\odot} \text{y}^{-1}$, see also Fuchs et al 2003).

But perhaps the best attempt so far to directly observe the mass donor has come from Gies et al (2002) who, using the interpretation that SS433 is a binary embedded in an expanding thick disc wind that explains the equatorial radio disc of Blundell et al (2001) and the stationary lines, also decided to observe SS433 spectroscopically at precessional phase, $\Psi \sim 0$, and in the blue where the expected high mass donor would be more easily detectable (and has historically been avoided due to the consequent need to use larger telescopes). During eclipse, Gies et al report the possible detection of (weak) spectral features that are typical of an A supergiant, which is consistent with photometry (Antokhina & Cherekpashchuk 1987; Goranskii et al 1997) that shows the donor to be cooler than the disc, which still dominates even in the blue. The velocities of these features and known orbital phase are combined with an assumed $e=0$ and Fabrika & Bychkova's K-velocity for HeII (assumed to represent the disc) to yield $q = M_2/M_X = 0.57$, $M_X = 11 \pm 5 M_{\odot}$, $M_2 = 19 \pm 7 M_{\odot}$, $R_2 = 31 \pm 3 R_{\odot}$ (assuming it is Roche-lobe filling), hence requiring a BH of similar mass to those found in the XRN. However, this result must be treated with caution until a full radial velocity curve has been obtained, but this will be extremely difficult given the large contribution from the bright and hot disc.

There also now exists a large database of SS433 V-band photometry (from 1979-1996) that Fabrika & Irmambetova (2002) have reanalysed by using (mostly) radio coverage to separate into active and passive states, which were then examined on both orbital and precessional phases. The most remarkable result is that the largest (optical/radio) flares occur almost entirely at orbital $\phi \sim 0.3$ (with a few at ~ 0.8), which implies a non-circular orbit! However, the well-known nodding motions in the jet (Katz et al 1982 [141]) set an independent upper limit of $e < 0.05$, but Fabrika & Irmambetova point out that an eccentricity as small as $e \simeq 0.01$ would be enough to modulate the Roche volume and thereby perturb the disc; it being the disc, and not \dot{M} which is already extremely high, that will modulate the flux, following an ~ 1 d delay in propagating the \dot{M} change through the disc. Such a small value of e would be undetectable in current optical spectroscopic studies.

5.3.13.2 *Cyg X-3: a Wolf-Rayet-BH X-ray binary*

Cygnus X-3 is a bright HMXB with the exceptionally short P_{orb} of 4.8h. It is also a strong radio source showing extensive outbursts associated with mass ejection events in a relativistic jet (Geldzahler et al, 1983). Because of its high extinction, it took the advent of IR spectroscopy to identify the nature of the mass donor when van Kerkwijk et al (1992) showed the IR emission lines to be arising from the strong stellar wind of a Wolf-Rayet (WN7) star, the only one currently identified with an X-ray binary. Subsequently, van Kerkwijk (1993), van Kerkwijk et al (1996) and Fender et al (1999) carried out detailed studies of the IR line profiles and explained the double and P-Cygni shapes to be associated with the high \dot{M} from the WR star and *not* the jets. Mid-IR ISOPHOT 2–12 μ observations (Koch-Miramond et al 2002) infer an expanding wind with $\dot{M} \sim 1.2 \pm 0.5 \times 10^{-4} M_{\odot} \text{y}^{-1}$ from the \sim WN8 donor.

X-ray spectroscopy by Paerels et al (2000) using the *Chandra* HETGS revealed a rich spectrum of photoionization-driven excited lines. An overall net redshift of

$\sim 750 \text{ km s}^{-1}$, independent of binary phase, was interpreted as an ionized region detached from the main mass outflow. Furthermore, detailed *Chandra* imaging (Heindl et al, 2003) revealed an X-ray structure extending some 16 arcsecs from the nucleus, which could be evidence for the strong stellar wind impacting the ISM, thereby producing bremsstrahlung X-ray emission.

The nature of the compact object within Cyg X-3 remains a puzzle. No direct pulsations have ever been detected which would indicate a NS. The presence of radio relativistic jets encourages many to include it in the galactic microquasar group, and hence, by implication, suggest that the compact object is a BH. And while van Kerkwijk (1993) and van Kerkwijk et al (1996) interpreted the IR line profile variations as due to geometrical variations in the X-ray illuminated hemisphere of the WR wind (supported by the correlation of line strength and wavelength shift), Schmutz et al (1996) obtained higher resolution spectra where the profiles did not follow the variation expected of this model. Instead, they interpret them as due to the straightforward orbital motion of the WR star which then implies $f(M)=2.3M_{\odot}$. With WN7 star masses in the range $10\text{--}50M_{\odot}$ (Cherepashchuk & Moffat 1994), or more conservatively $5\text{--}20M_{\odot}$ (Massey 1982), and i in the range $30\text{--}90^{\circ}$ then $M_X > 7M_{\odot}$, which makes Cyg X-3 an important system as potentially the *only* currently identified WR/BH system (although two further candidates have been proposed in the LMC, Wang 1995, and in IC10, Clark & Crowther 2003), suggesting either a rare formation mechanism (e.g. van den Heuvel & de Loore 1973) or a short lifetime, which might be expected given the extremely high inferred \dot{M} . A more detailed analysis of the Fender et al data is given in Hanson et al (2000) which reveals, during outburst, an absorption component in HeI which is out of phase (by ~ 0.25 cycle) with the emission lines. They present a compelling case, for interpreting this as the radial velocity curve of the WR wind, yielding similar masses to those above.

5.3.13.3 *Cir X-1: HMXB or LMXB?*

Since its discovery in the early 1970's (Margon et al. 1971) the nature of the X-ray binary Cir X-1 has remained elusive, in spite of the known $P_{orb}=16.6\text{d}$ inferred from the modulation of the X-ray (Kaluzienski et al. 1976), near-IR (Glass 1994) and radio fluxes (Haynes et al. 1978) and the discovery of Type I X-ray bursts identifying the compact object as a NS (Tennant et al. 1986). High extinction has made spectral classification of the donor impossible: the best optical spectra to date are dominated by asymmetric, H α , HeI emission lines (Johnston et al. 1999; Johnston et al. 2001), with no photospheric features evident.

The lack of spectral type has made determination of the accretion mode difficult. Murdin et al. (1980) interpreted the X-ray and radio modulations as evidence for direct accretion from a massive stellar wind. Indeed the X-ray behaviour of Cir X-1 is similar to that of the 16.65d BeX A0538-66, in which wind-fed accretion is enhanced by pseudo Roche-lobe overflow at periastron passage (Charles et al. 1983).

Conversely, Johnston et al. (1999) suggest that a similar scenario is also possible with an intermediate mass ($3\text{--}5M_{\odot}$) companion. Furthermore, spectral-timing studies of Cir X-1 with RXTE/PCA (Shirey et al. 1999) show Z-source X-ray QPO behaviour, suggesting an LMXB classification (cf. van der Klis 1995). However, the proposed association with the young SNR G321.9-0.3, which would support a low-

mass classification has recently been disproved by a proper motion study (Mignani et al. 2002). Detailed IR spectroscopy (Clark et al. 2003) reveals a spectrum that superficially resembles that of a high-luminosity mid-B supergiant, however it is concluded that the true spectrum of the donor remains obscured by the emission from the disc or accretion driven outflows.

Clearly a consensus on the nature of Cir X-1 has yet to be reached.

5.3.13.4 *CI Cam: a fast transient B[e] HMXB?*

In 1998 RXTE detected an extremely bright (~ 2 Crab) new transient, J0421+560 (Smith et al, 1998) with a positional error circle that included the known, bright ($V \sim 11$) B[e] supergiant CI Cam. Optical spectroscopy at the time of outburst (Wagner & Starrfield 1998) revealed HeII emission superposed on the already rich emission line spectrum, which strongly suggested CI Cam was responsible for the X-ray source. Contemporaneous photometry (Hynes et al, 2002c) revealed CI Cam to be 2-3 magnitudes brighter than usual, and this combined with a radio detection by Hjellming & Mioduszewski (1998) confirmed the identification. However, the extremely rapid decay (~ 2 d) of the outburst was highly unusual, with only V4641 Sgr of the XRN described earlier exhibiting similarly fast variations.

Hynes et al (2002c) have presented a major review of this system, but there are still some major questions left unanswered. It has been demonstrated that CI Cam is a sgB[e] which underwent a major mass outburst phase, and that this ejected material interacted with a compact object (presumed to be a neutron star or black hole). The ejected mass underwent supercritical accretion on to the compact object resulting in the subsequent ejection of much of the material. This thereby gave rise to the observed radio emission and the broadened optical emission lines. Hynes et al, however, point out that there is, so far, no evidence of binarity in this system and that, although unlikely, the intriguing possibility exists that the interaction with the compact object was merely a chance encounter between two unbound objects. CI Cam's high luminosity makes it a Galactic counterpart to the Magellanic Cloud sgB[e] stars, but it does not fit at all well into the classical Be/OB HMXB classification, and it has even been suggested (Ishida et al 2004) that the variable soft X-ray component might indicate that it is analogous to the supersoft sources (chapter 11) which would make the compact object a white dwarf.

Acknowledgments

We are grateful to our many colleagues who commented on earlier drafts of the manuscript and sent information in advance of publication. In particular, we would like to thank Reba Bandyopadhyay, Jorge Casares, Mike Garcia, Dawn Gelino, Rob Hynes, Lydie Koch-Miramond, Tariq Shahbaz, and John Tomsick.

References

- Alcock, C. et al. 1996, ApJ, 461, 84.
 Alcock, C. et al. 2001, MNRAS 321, 678.
 Antokhina, E.A. & Cherepashchuk, A.M. 1985, Soviet Astron., 11, 4.
 Antokhina, E.A. & Cherepashchuk, A.M. 1987, Soviet Astron., 31, 295.
 Augusteijn, T. et al. 2001, A&A, 375, 447.
 Avni Y., & Bahcall J. N. 1975, ApJ, 197, 675.
 Avni Y. 1978, in *Physics and Astrophysics of Neutron Stars and Black Holes*, eds. Giacconi & Ruffini (Amsterdam: North-Holland), 42.
 Bałucińska-Church M. et al. 2000 MNRAS, 311, 861.
 Bandyopadhyay, R. et al. 1997, MNRAS, 285, 718.
 Bandyopadhyay, R.M. et al. 1999, MNRAS, 306, 417.
 Bandyopadhyay, R.M. et al. 2002, ApJ, 570, 793.
 Bandyopadhyay, R.M. et al. 2003, MNRAS, 340, L13.
 Barziv, O. et al. 2001, A&A 377, 925.
 Beekman, G. et al. 1996, MNRAS, 281, L1.
 Beekman, G. et al. 1997, MNRAS, 290, 303.
 Beer, M.E. & Podsiadlowski, Ph. 2002, MNRAS, 331, 351.
 Berriman, G. et al. 1985, MNRAS, 217, 327.
 Bhattacharya, D. 2002, J.Ap.A., 23, 67.
 Bildsten, L. 2002, ApJ, 577, L27.
 Bildsten, L. & Chakrabarty, D. 2001, ApJ, 557, 292.
 Bildsten, L. & Rutledge, R.E. 2000, ApJ, 541, 908.
 Bildsten, L. et al. 1997, ApJS, 113, 367.
 Blaauw, A. 1961, Bull. Astron. Inst. Netherlands, 15, 265.
 Blundell, K.M. et al. 2001, ApJ, 562, L79.
 Bradshaw, C.F. et al. 1999, ApJ, 512, L121.
 Brandt, W.N. et al. 1995, MNRAS, 277, L35.
 Brocksopp, C. et al. 1999, A&A, 343, 861.
 Burderi, L. et al. 2003, A&A (in press), astro-ph/0305157.
 Callanan, P.J. et al. 1992, MNRAS, 259, 395.
 Callanan, P.J. et al. 2002, ApJ, 574, L143.
 Callanan, P.J. et al. 1995, PASJ, 47, 153.
 Cannizzo, J.K. 1998, ApJ, 494, 366.
 Casares, J. et al. 1992, Nature, 355, 614.
 Casares, J. & Charles, P.A. 1994, MNRAS, 271, L5.
 Casares, J. et al. 1995, MNRAS, 274, 565.
 Casares, J. et al. 1997, New Astron., 1, 299.
 Casares, J. et al. 2002, MNRAS, 329, 29.
 Casares, J. et al. 2003, ApJ, 590, 1041.
 Chakrabarty, D. & Morgan, E.H. 1998, Nature, 394, 346.
 Chakrabarty, D. & Roche, P. 1997, ApJ, 489, 254.
 Charles, P.A. et al. 1983, MNRAS, 202, 657.
 Charles, P.A. & Naylor, T. 1992, MNRAS, 255, L6.
 Charles, P.A. 2001, in *Black Holes in Binaries and Galactic Nuclei*, eds Kaper, van den Heuvel & Woudt, (Springer).
 Chen, W. et al. 1993, ApJ, 408, L5.
 Chen, W. et al. 1997, ApJ, 491, 312.
 Cherepashchuk, A.M. & Moffat, A.F.J. 1994, ApJ, 424, L53.
 Chou, Y. et al. 2001, ApJ, 549, 1135.
 Clark, J.S. et al. 1999, A&A 348, 888.
 Clark, J.S. et al. 2001, A&A 380, 615.
 Clark, J.S. et al. 2002, A&A 392, 909.
 Clark, J.S. & Crowther, P.A. 2003, A&A (in press).
 Clark, J.S. et al. 2003 A&A 400, 655.
 Covino, S. et al. 2001, A&A 374, 1009.
 Coe, M.J. et al. 1994, A&A, 289, 784.
 Coe, M.J. et al. 2002, MNRAS 332, 473.
 Coe, M.J. & Orosz J.A. 2000, MNRAS 311, 169.
 Corbet, R.H.D. 1986, MNRAS 220, 1047.
 Cowley, A.P. et al. 2002, AJ, 123, 1741.
 Cutler, E.P. et al. 1986, ApJ, 300, 551.
 Dachs, J. & Wamsteker, W. 1982, A&A, 107, 240.
 della Valle, M. et al. 1997, A&A, 318, 179.
 Deutsch, E.W. et al. 1999, ApJ, 524, 406.
 d'Odorico, S. et al. 1991, Nature, 353, 329.
 Eggleton, P.P. 1983, ApJ, 268, 368.
 Eracleous, M. & Horne, K. 1996, ApJ, 471, 427.
 Ergma, E. & Sarna, M.J. 2001, A&A, 374, 195.
 Eyles, C.J. et al. 1975, Nature, 254, 577.
 Fabrika, S.N. & Bychkova, L.V. 1990, A&A, 240, L5.
 Fabrika, S. & Irsmambetova, T. 2002, in *New Views on Microquasars*, p268. Center for Space Physics, eds Durouchoux, Fuchs & Rodriguez (Kolkata, India).
 Fender, R.P. et al. 1999, MNRAS, 308, 473.
 Filippenko, A.V. et al. 1995a, ApJ, 455, L139.
 Filippenko, A.V. et al. 1995b, ApJ, 455, 614.
 Filippenko, A.V. et al. 1997, PASP, 109, 461.
 Filippenko, A.V. et al. 1999, PASP, 111, 969.
 Filippenko, A.V. & Chornock, R. 2001, IAUC7644.
 Fomalont, E.B. et al. 2001, ApJ, 558, 283.
 Fuchs, Y. et al. 2003, in *New Views on Microquasars*, p.269 Center for Space Physics, eds Durouchoux, Fuchs & Rodriguez (Kolkata, India) astro-ph/0208432.
 Galloway, D.K. et al. 2002, ApJ, 576, L137.

- Garcia, M.R. et al. 1992, AJ, 103, 1325.
 Geldzahler, B.J. et al. 1983, ApJ, 273, L65.
 Gelino, D.M. 2003 (in prep.)
 Gelino, D.M. & Harrison, T.E. 2003, ApJ (in press), astro-ph/0308490.
 Gelino, D.M. et al. 2001a, AJ, 122, 971.
 Gelino, D.M. et al. 2001b, AJ, 122, 2668
 Gies, D.R. et al. 2002, ApJ, 578, L67.
 Giles, A.B. et al. 1999, MNRAS, 304, 47.
 Glass, I. S. 1994, MNRAS, 268, 742.
 Goranskii, V.P. et al. 1998, Astron. Rep., 42, 336.
 Goranskii, V.P. et al. 1997, Astron. Rep., 41, 656.
 Gottlieb, E.W. et al. 1975, ApJ, 195, L33.
 Greene, J. et al. 2001, ApJ, 554, 1290.
 Greiner, J. et al. 1998, New Astron. Rev., 42, 597.
 Greiner, J. et al. 2001 Nature, 414, 522.
 Grindlay, J.E. et al. 1988, ApJ, 334, L25.
 Grindlay, J.E. 1989, in Proc. 23rd ESLAB Symposium on *Two Topics in X-ray Astronomy*, p121. (ESA SP)
 Hakala, P.J. et al. 1998, A&A, 333, 540.
 Hakala, P.J. et al. 1999, MNRAS, 306, 701.
 Hameury, J.-M. et al. 1997, ApJ, 489, 234.
 Hanson, M.M. et al. 2000, ApJ, 541, 308.
 Hanuschik, R.W. et al. 1988, 189, 147.
 Hanuschik, R.W. 1996, A&A, 308, 170.
 Harlaftis, E.T. et al. 1997, MNRAS, 285, 673.
 Harlaftis, E.T. et al. 1996, PASP, 108, 762.
 Harlaftis, E.T. et al. 1997, AJ, 114, 1170.
 Harlaftis, E.T. et al. 1999, A&A, 341, 491.
 Haswell, C.A. et al. 2001, MNRAS, 321, 475.
 Haswell, C.A. et al. 2002, MNRAS, 332, 928.
 Haynes, R.F. et al. 1978, MNRAS, 185, 661.
 Heindl, W.A. et al. 2003, ApJ 588, 97.
 Hellier, C. 2000, New Astron. Rev., 44, 131.
 Herrero, A. et al. 1995, A&A, 297, 556.
 Hillier, D.J. & Miller, D.L. 1998, ApJ, 496, 407.
 Hjellming, R.M. 1978, ApJ, 221, 225.
 Hjellming, R.M. & Mioduszewski, A.J. 1998, IAUC 6862.
 Homer, L. et al. 2001a, MNRAS, 325, 1471.
 Homer, L. et al. 2001b, MNRAS, 322, 827.
 Horne K. 1999a in *Quasars and Cosmology* ASP Conf Series 162, p189 eds Ferland & Baldwin (ASP, San Francisco).
 Horne K. 1999b in *Magnetic Cataclysmic Variables* ASP Conf Series 157, p349 eds Mukai & Hellier (ASP, San Francisco).
 Hutchings, J.B. et al. 1983, ApJ, 275, L43.
 Hutchings, J.B. et al. 1987, AJ, 94, 340.
 Hynes, R.I. et al. 1998, MNRAS, 299, L37.
 Hynes, R.I. et al. 2000, ApJ, 539, L37.
 Hynes, R.I. et al. 2001a, MNRAS, 324, 180.
 Hynes, R.I. et al. 2001b, in *Astrotomography, Indirect Imaging Methods in Observational Astronomy* Lecture Notes in Physics, Vol. 573, p378 eds Boffin, Steeghs & Cuypers, (Springer).
 Hynes, R.I. et al. 2002a, MNRAS, 330, 1009.
 Hynes, R.I. et al. 2002b, MNRAS, 331, 169.
 Hynes, R.I. et al. 2002c, A&A, 392, 991.
 Hynes, R.I. et al. 2003a, MNRAS, 345, 292.
 Hynes, R.I. et al. 2003b, ApJ, 583, L95.
 in't Zand, J.J.M. et al. 1998, A&A, 331, L25.
 Ishida, M. et al. 2004, ApJ, 601, in press.
 Israelian, G. et al. 1999, Nature, 401, 142.
 Jablonski, F.J. et al. 1997, ApJ, 482, L171.
 Johnston, H.M. et al. 1999, MNRAS, 308, 415.
 Johnston, H.M. et al. 2001, MNRAS, 328, 1193.
 Jonker, P.G. et al. 2000, MNRAS, 315, L57.
 Kaiser, C.R. & Hannikainen, D.C. 2002, MNRAS, 330, 225.
 Kanbach, G. et al. 2001, Nature, 414, 180.
 Kaluzienski, L.J. et al. 1976, ApJ, 208, L71.
 Kaper, L. et al. 1997, A&A 327, 281.
 Katz, J.I. et al. 1982, ApJ, 260, 780.
 King, A.R. et al. 1996, ApJ, 464, L127.
 King, A.R. & Ritter, H. 1998, MNRAS, 293, L42. .
 Kirsch, M.G.F. & Kendziorra, E. 2003, ATel, 148.
 Kolb, U. et al. 1997, ApJ, 485, L33.
 Kolb, U. 1998, MNRAS, 297, 419.
 Kong, A.K.H. et al. 2002, MNRAS, 329, 588.
 Kuiper, L. et al. 1988, A&A, 203, 79.
 Kuulkers, E. 1998, New Astron. Rev., 42, 613.
 LaSala, J. & Thorstensen, J.R. 1985, AJ, 90, 2077.
 LaSala, J. et al. 1998, MNRAS, 301, 285.
 Lasota, J.-P. 2000, A&A, 360, 575.
 Lasota, J.-P. 2001, New Astron. Rev., 45, 449.
 Laycock S.G.T. et al, 2003 (in prep.)
 Liu, Q.Z. et al. 2000, A&A Suppl., 147, 25.
 Liu, Q.Z. et al. 2001, A&A, 368, 1021.
 Maeder, A. et al. 1999, A&A 346, 459.
 Maragoudaki, F. et al. 2001, A&A 379, 864.
 Margon, B. et al. 1971, ApJ, 169, L23.
 Margon, B. 1984, ARAA, 22, 507.
 Markwardt, C.B. et al. 2002, ApJ, 575, L21.
 Markwardt, C.B. et al. 2003, ATel, 164.
 Marsh, T.R. 2001, in *Astrotomography, Indirect Imaging Methods in Observational Astronomy* Lecture Notes in Physics, 71 eds Boffin, Steeghs & Cuypers, (Springer).
 Marsh, T.R. et al. 1994, MNRAS, 266, 137.
 Martin, A.C. et al. 1995, MNRAS, 274, L46.
 Martín, E.L. et al. 1992, Nature, 358, 129.
 Martín, E.L. et al. 1994, A&A, 291, L43.
 Martín, E.L. et al. 1995, A&A, 303, 785.
 Martín, E.L. et al. 1996, New Astron., 1, 197.
 Masetti, N. et al. 2002, A&A, 382, 104.

- Massey, P. 1982, IAU Symp. 99, 251.
- McClintock, J.E. & Remillard, R.A. 1986, ApJ, 308, 110.
- McClintock, J.E. & Remillard, R.A. 1990, ApJ, 350, 386.
- McGowan, K.E. & Charles, P.A. 2003, MNRAS 339, 748.
- Meyssonnier, N. & Azzopardi, M. 1993, A&AS 102, 451.
- Mignani, R.P. et al. 2002, A&A, 386, 487
- Mineshige, S. et al. 1992, PASJ, 44, L15.
- Mirabel, I.F. & Rodriguez, L.F. 1999, ARAA, 37, 409.
- Mukai, K. et al. 2001, ApJ, 561, 938.
- Murdin, P. et al. 1980, A&A, 87, 292.
- Murray, J. 2000, MNRAS, 314, L1.
- Nagase, F. 1989, PASJ, 41, 1.
- Naylor, T. et al. 1991, MNRAS, 252, 203.
- Negueruela, I. 1998, A&A, 338, 50.
- Negueruela, I. & Coe M.J. 2002, A&A 385, 517.
- O'Donoghue, D. & Charles, P.A. 1996, MNRAS, 282, 191.
- Ogilvie, G.I. & Dubus, G. 2001, MNRAS, 320, 485.
- Okazaki, A. T. & Negueruela, I. 2001, A&A 377, 161.
- Orosz, J.A. et al. 1994, ApJ, 436, 848.
- Orosz, J.A. et al. 1996, ApJ, 468, 380.
- Orosz, J.A. & Bailyn C.D. 1997, ApJ, 477, 876 (and ApJ, 482, 1086).
- Orosz, J.A. et al. 1997, ApJ, 478, L83.
- Orosz, J.A. & Kuulkers E. 1999, MNRAS, 305, 132.
- Orosz, J.A. 2001, Astron.Tel. No. 67.
- Orosz, J.A. et al. 2001, ApJ, 555, 489.
- Orosz, J.A. et al. 2002a, ApJ, 568, 845.
- Orosz, J.A. et al. 2002b, BAAS, 201.1511.
- Orosz, J.A. 2003, Proc. IAU Symp. 212, eds. K.A. van der Hucht, A. Herrero & C. Esteban.
- Osaki, Y. 1985, A&A, 144, 369.
- Paczynski, B. 1971, ARAA, 9, 183.
- Paerels, F. et al. 2000, ApJ, 533, 135.
- Parmar, A.N. & White, N.E. 1988, Mem.It.Astr.Soc., 59, 147.
- Patterson, J. 1995, PASP, 107, 1193.
- Patterson, J. 1999, in *Close Binary Systems*, Frontiers Science Series, No. 26, p61 eds S. Mineshige & J.C. Wheeler.
- Patterson, J. 2001, PASP, 113, 736.
- Pavlenko, E.P. et al. 1996, MNRAS, 281, 1094.
- Pereira, M.G. et al. 1999 ApJ, 526, L105.
- Phillips, S.N. et al. 1999 MNRAS, 304, 839.
- Podsiadlowski, Ph. et al. 2002, ApJ, 567, 491.
- Popov, S.B. et al. 1998, Astron Reports, 42, 29.
- Putman, M.E. et al. 1998, Nature, 394, 752.
- Reig, P. & Roche, P. 1999, MNRAS, 306, 100.
- Remillard, R.A. et al. 1996, ApJ, 459, 226.
- Remillard, R.A. et al. 2000, IAUC 7389.
- Retter, A. et al. 2002, MNRAS, 330, L37.
- Roche, P. et al. 1998, IAUC 6885.
- Safi-Harb, S. 2003, in *New Views on Microquasars*, p243. Center for Space Physics, eds Durouchoux, Fuchs & Rodriguez (Kolkata, India).
- Samimi, J. et al. 1979, Nature, 278, 434.
- Sanwal, D. et al. 1996, ApJ, 460, 437.
- Schachter, J. et al. 1989, ApJ, 340, 1049.
- Schandl, S. & Meyer, F. 1994, A&A, 289, 149.
- Schmutz, W. et al. 1996, A&A, 311, L25.
- Shafter, A.W. et al. 1988, ApJ, 327, 248.
- Shahbaz, T. et al. 1993, MNRAS, 265, 655.
- Shahbaz, T. et al. 1994a, MNRAS, 268, 756.
- Shahbaz, T. et al. 1994b, MNRAS, 271, L10.
- Shahbaz, T. et al. 1996, MNRAS, 282, 977.
- Shahbaz, T. et al. 1997, MNRAS, 285, 607.
- Shahbaz, T. & Kuulkers, E. 1998, MNRAS, 295, L1.
- Shahbaz, T. et al. 1998, MNRAS, 301, 382.
- Shahbaz, T. et al. 1999a, A&A, 346, 82.
- Shahbaz, T. et al. 1999b, MNRAS, 306, 89.
- Shahbaz, T. et al. 2000, MNRAS, 314, 747.
- Shahbaz, T. et al. 2001, A&A, 376, L17.
- Shahbaz, T. et al. 2003, ApJ, 585, 443.
- Shirey, R.E. et al. 1999, ApJ, 517, 472.
- Smale, A.P. & Lochner, J.C. 1992, ApJ, 395, 582.
- Smith, D. & Dhillon, V.S. 1998, MNRAS, 301, 767.
- Smith, D. et al. 1998, IAUC 6855.
- Soria, R. et al. 1998, ApJ, 495, L95.
- Soria, R. et al. 1999, MNRAS, 309, 528.
- Stanimirovic, S. et al. 1999, MNRAS, 302, 417.
- Staveland-Smith, L. et al. 1997, MNRAS, 289, 225.
- Steenhals, D. & Casares, J. 2002, ApJ, 568, 273.
- Stella, L. et al. 1986, ApJ, 308, 669.
- Sunyaev, R.A. et al. 1992, ApJ, 389, L75.
- Tanaka, Y. & Shibasaki, N. 1996, ARAA, 34, 607.
- Telting, J.H. et al. 1998, MNRAS, 296, 785.
- Tennant, A. F. et al. 1986, MNRAS, 221, 27.
- Thorsett, S.E. & Chakrabarty, D. 1999, ApJ, 512, 288.
- Tjemkes, S.A. et al. 1986, A&A, 154, 77.
- Tomsick, J.A. et al. 1999, ApJ, 521, 341.
- Tomsick, J.A. et al. 2001, ApJ, 559, L123.
- Tomsick, J.A. et al. 2002, ApJ, 581, 570.
- Torres, M.A.P. et al. 2002, MNRAS, 334, 233.
- Udalski A. et al. 1997, Acta Astron., 47, 319.
- van Bever, J. & Vanbeveren, D. 1997, A&A, 322, 116.
- van den Heuvel, E.P.J. 1983, in *Accretion*

- driven stellar X-ray sources*, eds Lewin & van den Heuvel (CUP).
- van den Heuvel, E.P.J. & de Loore, C. 1973, A&A, 25, 387.
- van der Hooft, F. et al. 1997, MNRAS, 286, L43.
- van der Hooft, F. et al. 1998, A&A, 329, 538.
- van Kerkwijk, M.H. et al. 1992, Nature, 355, 703.
- van Kerkwijk, M.H. et al. 1996, A&A, 314, 521.
- van Kerkwijk, M.H. 1993, A&A, 276, L9.
- van der Klis, M. 1995, in *X-Ray Binaries*, eds Lewin, van Paradijs & van den Heuvel, 252 (CUP).
- van Loon, J.Th. et al. 2001, A&A 375, 498.
- van Paradijs, J. & McClintock, J.E. 1994, A&A, 290, 133.
- van Paradijs, J. & McClintock, J.E. 1995, in *X-Ray Binaries*, eds. Lewin, van Paradijs & van den Heuvel, 58 (CUP).
- van Paradijs, J. 1998, in *The Many Faces of Neutron Stars*, eds. Buccheri, van Paradijs & Alpar (Kluwer).
- Verbunt, F. & van den Heuvel, E.P.J. 1995, in *X-ray Binaries*, eds. Lewin, van Paradijs & van den Heuvel (CUP).
- Wachter, S. 1998, PhD thesis, University of Washington, Seattle.
- Wachter, S. et al. 2002, ApJ, 568, 901.
- Wade, R.A. & Horne, K. 1988, ApJ, 324, 411.
- Wagner, R.M. & Starrfield, S.G. 1998, IAUC 6857.
- Wagner, R.M. et al. 1992, ApJ, 401, 97.
- Wagner, R.M. et al. 2001, ApJ, 556, 42.
- Walter, F.M. et al. 1982, ApJ, 253, L67.
- Wang, Q.D. 1995, ApJ, 453, 783.
- Warner, B. 1995, in *Cataclysmic Variables*, 117 (CUP).
- Webb, N.A. et al. 2000, MNRAS, 317, 528.
- White, N.E. et al. 1995, in *X-ray Binaries*, eds. Lewin, van Paradijs & van den Heuvel (CUP).
- White, N.E. & van Paradijs, J. 1996, ApJ, 473, L25.
- Whitehurst, R. & King, A.R. 1991, MNRAS, 249, 25.
- Wijers, R.A.M.J. & Pringle, J.E. 1999, MNRAS, 308, 207.
- Wijnands, R. & van der Klis, M. 1998, ApJ, 507, L63.
- Wilson, C.A. et al. 2002, ApJ, 570, 287.
- Zurita, C. et al. 2000, MNRAS, 316, 137.
- Zurita, C. et al. 2002a, MNRAS, 333, 791.
- Zurita, C. et al. 2002b, MNRAS, 334, 999.